Colloquium: Atomtronic circuits: From many-body physics to quantum technologies

Luigi Amico*

Quantum Research Centre, Technology Innovation Institute, Abu Dhabi 9639, United Arab Emirates, INFN-Sezione di Catania, Via Santa Sofia 64, 95127 Catania, Italy, Centre for Quantum Technologies, National University of Singapore, 3 Science Drive 2, Singapore 117543, Singapore, and MajuLab, CNRS-UNS-NUS-NTU International Joint Research Unit, UMI 3654, Singapore 117543, Singapore

Dana Anderson

Department of Physics and JILA, University of Colorado, Boulder, Colorado 80309-0440, USA

Malcolm Boshier

MPA Division, Los Alamos National Laboratory, Los Alamos, New Mexico 87545, USA

Jean-Philippe Brantut

Institute of Physics, EPFL, 1015 Lausanne, Switzerland

Leong-Chuan Kwek

Centre for Quantum Technologies, National University of Singapore, 3 Science Drive 2, Singapore 117543, Singapore, MajuLab, CNRS-UNS-NUS-NTU International Joint Research Unit, UMI 3654, Singapore 117543, Singapore, and Institute of Advanced Studies, Nanyang Technological University, 60 Nanyang View, Singapore 639673, Singapore

Anna Minguzzi

Université Grenoble-Alpes and CNRS, LPMMC, F-38000 Grenoble, France

Wolf von Klitzing

Institute of Electronic Structure and Laser, Foundation for Research and Technology–Hellas, Crete, Heraklion 70013, Greece

(published 18 November 2022)

Atomtronics is an emerging field that aims to manipulate ultracold atom moving in matter-wave circuits for fundamental studies in both quantum science and technological applications. In this Colloquium, recent progress in matter-wave circuitry and atomtronics-based quantum technology is reviewed. After an introduction to the basic physical principles and the key experimental techniques needed to realize atomtronic systems, the physics of matter waves in simple circuits such as ring traps and two-terminal systems is described. The main experimental observations and outstanding questions are discussed. Also presented are possible applications to a broad range of quantum technologies, from quantum sensing with atom interferometry to future quantum simulation and quantum computation architectures.

DOI: 10.1103/RevModPhys.94.041001

CONTENTS

*On leave from Dipartimento di Fisica e Astronomia, Via Santa Sofia 64, 95127 Catania, Italy.

I. INTRODUCTION

Atomtronics is the emerging quantum technology of matter-wave circuits that coherently guide propagating ultracold atoms (Amico, Osterloh, and Cataliotti, 2005; Seaman *et al.*, 2007; Amico *et al.*, 2017, 2021). Developing and applying such circuits has been a goal of cold-atom physics for decades; see Müller *et al.* (1999), Dekker *et al.* (2000), Dumke *et al.* (2002), Leanhardt *et al.* (2002), and Schneble *et al.* (2003). Realizing this vision was an important motivation for the invention and development of atom-chip technology at the beginning of this century (Schmiedmayer, 1995b; Schmiedmayer and Scrinzi, 1996a, 1996b; Denschlag *et al.*, 1999; Denschlag, Cassettari, and Schmiedmayer, 1999). While this approach has not yet demonstrated coherent propagation of guided matter waves, there is an extensive body of work on the coherent manipulation of trapped clouds of ultracold atoms on atom chips that provides a foundation for the more recent work discussed here. This research was reviewed by Folman *et al.* (2002), Reichel (2002), Fortágh and Zimmermann (2007), Reichel and Vuletić (2011), and Keil *et al.* (2016). In the implementations of atomtronic circuits that have been realized to date, matter waves travel in guides made of laser light or magnetic fields. These approaches offer highly controllable, flexible, and versatile platforms at the microscopic spatial scale (Henderson *et al.*, 2009; Rubinsztein-Dunlop *et al.*, 2017; Gauthier *et al.*, 2019). The quantum fluid flowing through atomtronic circuits is provided by ultracold atoms that can be fermions, bosons, or a mixture of the two species. Cold-atom quantum technology allows coherent matter-wave manipulations with unprecedented control and precision over a wide range of spatial lengths and physical conditions (Dalfovo *et al.*, 1999; Cornell and Wieman, 2002; Ketterle, 2002; Bloch, 2005).

Atomtronic circuits are suitable as cold-atom quantum simulators (Dowling and Milburn, 2003; Bloch, 2005; Buluta and Nori, 2009; Cirac and Zoller, 2012; Lewenstein, Sanpera, and Ahufinger, 2012; Lamata *et al.*, 2014) in which matter-wave currents are harnessed as probes to explore the physics of the system. In this way, important problems in fundamental quantum science, such as superfluidity, strong correlations in extended systems, topological aspects in quantum matter, quantum transport, and various mesoscopic effects, can be studied from a new perspective (Stadler *et al.*, 2012; Husmann *et al.*, 2015; Valtolina *et al.*, 2015; Krinner *et al.*, 2016; Burchianti *et al.*, 2018; Del Pace *et al.*, 2021).

At the same time, atomtronic circuits play an important role in applied science and technology. Like electronic devices, atomtronic circuits operate over a separation of timescales and length scales between devices and leads. This permits the construction of standardized functional units connected to each other by waveguides acting as wires. Atomtronic counterparts of known electronic or quantum electronic components have been the first developments in the field. Some examples include atomtronic amplifiers, diodes, switches, batteries, and memories (Seaman *et al.*, 2007; Stickney, Anderson, and Zozulya, 2007; Pepino *et al.*, 2009; Caliga *et al.*, 2016; Caliga, Straatsma, and Anderson, 2017; Anderson, 2021; Pepino, 2021). Moreover, cold-atom realizations of Josephson junctions have led to the fabrication and analysis of atomtronic superconducting quantum interference devices (SQUIDs) (Ramanathan *et al.*, 2011; Ryu *et al.*, 2013; Amico *et al.*, 2014; Eckel, Lee *et al.*, 2014; Jendrzejewski *et al.*, 2014; Aghamalyan *et al.*, 2015; Haug, Tan *et al.*, 2018). Atomtronics can also contribute to the field of quantum sensors (Cronin, Schmiedmayer, and Pritchard, 2009; Degen, Reinhard, and Cappellaro, 2017; Bongs *et al.*, 2019). Building on the pioneering demonstrations of compact atom interferometers using trapped Bose-Einstein condensates (BECs) (Schumm *et al.*, 2005; Günther *et al.*, 2007; Jo *et al.*, 2007; Böhi *et al.*, 2009; Riedel *et al.*, 2010), several solutions for compact atomtronic interferometers with enhanced

sensitivity to inertial forces and electromagnetic fields have been studied (Wang *et al.*, 2005; Wu, Su, and Prentiss, 2007; Burke and Sackett, 2009; McDonald, Keal *et al.*, 2013; McDonald *et al.*, 2014; Ryu and Boshier, 2015; Akatsuka, Takahashi, and Katori, 2017; Qi *et al.*, 2017; Moan *et al.*, 2020; Kim *et al.*, 2022; Krzyzanowska *et al.*, 2022. Finally, we observe that the aforementioned specific properties of coherence, control, and flexibility characterizing ultracold matter-wave circuits can enable devices with no direct analog in electronics or photonics technology. Proofs of concept built on features inherent to specified microscopic implementations and combined with specifically suited enabling technologies have recently been considered (Aghamalyan, Amico, and Kwek, 2013; Amico *et al.*, 2014; Chetcuti, Haug *et al.*, 2022; Kim *et al.*, 2022; Krzyzanowska *et al.*, 2022; Lau *et al.*, 2022; Naldesi *et al.*, 2022).

In this Colloquium, we provide an accessible review of the atomtronics field for a broad, educated audience of researchers. For a more technical discussion of some of the most recent developments, see the road map article by Amico *et al.* (2021). The Colloquium is organized as follows: In Sec. II, we discuss the state of the art in optical and magnetic trapping technologies that lead to a variety of circuits. In Sec. III, we focus on the coherent flow in simple atomtronic networks of mesoscopic size. In that section, we bridge many-body models with persistent currents and two-terminal transport through a mesoscopic channel. In Sec. IV, we describe some of the components that have been studied and developed thus far. Finally, we conclude and provide an outlook in Sec. V.

II. TRAPS AND GUIDES

Atomotronics has been made possible by the ability to trap matter waves of coherent cold atoms in complex smooth potentials in which matter waves can be feasibily created, guided, and manipulated in a controllable and flexible fashion. These potentials are produced either by optical fields that exert forces on atoms through their polarizability or by magnetic fields that create forces on atomic magnetic dipoles.

A. Optical potentials

The formation of optical potentials through static or dynamic laser beams is a mature technology for the realization of atomtronic circuitry. The flexible potentials can have an almost arbitrary complexity in both space and time domains.

Optical manipulation of ultracold atoms is based on the electric dipole interaction between the atoms and the laser beam. When the laser frequency ω is far detuned from an atomic transition of the frequency ω_0, the interaction energy takes the form of an optical dipole potential $U(\mathbf{r}) = -(3\pi c^2/2\omega_0^3)(\Gamma/\Delta)I(\mathbf{r})$, where $\Delta = \omega - \omega_0$ is the detuning, Γ is the natural decay rate of the population of the excited state, and $I(\mathbf{r})$ is the position-dependent laser intensity. This dipole force can be attractive ($\Delta < 0$ or "red detuned") or repulsive ($\Delta > 0$ or "blue detuned") (Grimm, Weidemüller, and Ovchinnikov, 2000). The detuning should be large enough that spontaneous scattering is negligible on the timescale of the experiment.

1. Static laser beams

Waveguides supporting a coherent propagation of matter waves must be smooth to avoid excitations out of the guide ground state to higher modes and must be stable because fluctuations in the potential cause fluctuations in the phase accumulated by the matter wave. A collimated laser beam is a straightforward solution to this problem. The first guides for cold, noncondensed atoms used the evanescent field of blue-detuned light propagating in a hollow optical waveguide (Renn *et al.*, 1996; Müller, Cornell, Anderson, and Abraham, 2000; Rhodes *et al.*, 2002). This is followed by the introduction of traps and guides based on hollow blue-detuned laser beams created with doughnut or Laguerre-Gaussian transverse modes that removed the need for a material optical guide (Kuga *et al.*, 1997). This approach enabled the creation of the first waveguide for a BEC (Bongs *et al.*, 2001). When the Laguerre-Gaussian beam is tightly focused, the optical dipole potential becomes more like a toroidal trap (Olson *et al.*, 2007) than a waveguide. Waveguide potentials can also be realized with Bessel beams (Arlt, Hitomi, and Dholakia, 2000).

The red-detuned collimated laser beam is a simpler technology for creating atomtronic waveguides when spontaneous emission is sufficiently small. An early example of this approach was the realization of a simple beam splitter for propagating cold thermal atoms with a pair of crossed red-detuned laser beams (Houde, Kadio, and Pruvost, 2000). Subsequent demonstrations included coherent propagations of BEC matter wave packets to realize a Mach-Zehnder atom interferometer (McDonald, Keal *et al.*, 2013; Kim *et al.*, 2022), a beam splitter for BECs (Gattobigio *et al.*, 2012), and a waveguide Sagnac atom interferometer (Krzyzanowska *et al.*, 2022). Red-detuned collimated lasers are also used to guide the matter wave produced by an atom laser (Guerin *et al.*, 2006; Couvert *et al.*, 2008; Dall *et al.*, 2010). A recent development is the use of clipped Gaussian beams to create elongated trapping and guiding potentials (Lim *et al.*, 2021).

Besides the previously mentioned standard approaches, microfabricated optical elements (Birkl *et al.*, 2001), arrays of microlenses (Dumke *et al.*, 2002), and the application of conical refraction in a biaxial crystal (Turpin *et al.*, 2015) have been proposed as sophisticated routes to realize complex circuits. Standing waves of laser light impressed on a collimated laser waveguide have been shown to form a distributed Bragg reflector (Fabre *et al.*, 2011). Pulsed optical standing waves are also employed as beam splitters (Wang *et al.*, 2005; Wu *et al.*, 2005; Kim *et al.*, 2022; Krzyzanowska *et al.*, 2022).

2. Time-averaged optical potentials

Optical dipole potentials based on static laser beams are cylindrically symmetric, and they can have no time dependence beyond a scaling of the trap strength. This shortcoming provided motivation for the development of time-averaged optical potentials. As with the previously discussed guides, the initial experiments following this approach used noncondensed thermal atoms, confining them to box and stadium potentials with walls formed by a blue-detuned laser beam that is rapidly scanned with a pair of acousto-optic deflectors

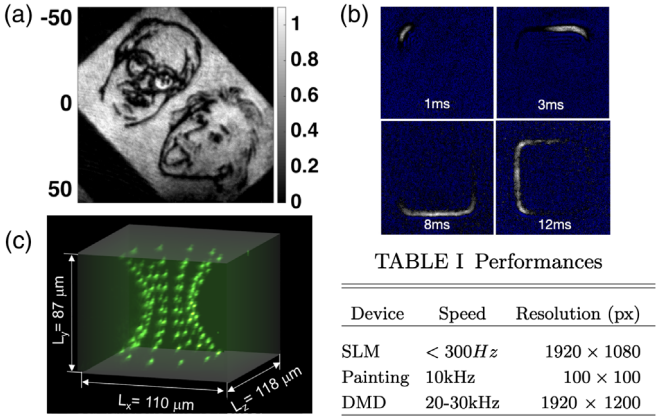

TABLE I Performances

Device	Speed	Resolution (px)
SLM	$< 300Hz$	1920×1080
Painting	10kHz	100×100
DMD	20-30kHz	1920×1200

FIG. 1. Bose-Einstein condensate trapped in a potential made by (a) DMD, length scales in micrometers, (b) painting technique (dimension of each image is 70×70 μm), and (c) SLM. The embedded table compares the performances of the devices in terms of refreshing time, resolution, and diffraction efficiency. (a) Adapted from Gauthier *et al.*, 2016. (b) Adapted from Ryu and Boshier, 2015. (c) Adapted from Barredo *et al.*, 2018.

(Friedman *et al.*, 2001; Milner *et al.*, 2001). While early experiments on trapping BECs in multiple wells, formed by rapidly switching the position of a single red-detuned laser, found that the condensates are heated (Onofrio *et al.*, 2000), that issue is absent from later work in which a time-averaged tightly focused laser beam "painted" a desired potential on a canvas provided by a light sheet that confined atoms to a horizontal plane. This "painted potential" (Schnelle *et al.*, 2008; Henderson *et al.*, 2009) is able to realize arbitrary and dynamic 2D matter waveguide structures; see Fig. 1(a). This includes the important case of toroidal potentials (Henderson *et al.*, 2009; Ryu, Henderson, and Boshier, 2014; Bell *et al.*, 2016), where, periodically reducing the intensity of the laser painting, the attractive potential creates movable repulsive barriers that can form Josephson junctions in an atom SQUID geometry (Ryu *et al.*, 2013; Ryu, Samson, and Boshier, 2020). Repulsive barriers can also be imposed on a trap by painting with a blue-detuned laser (Ramanathan *et al.*, 2011; Wright *et al.*, 2013a). A significant advantage of this approach is that a suitable modulation of the tweezer beam intensity as it paints the atomtronic circuit can flatten out any imperfections in the potential (Ryu and Boshier, 2015; Bell *et al.*, 2016), thus enabling the creation of waveguides smooth enough to support single mode propagation and to realize the first coherent beam splitter for propagating matter waves (Ryu and Boshier, 2015).

While painting has the advantages of making efficient use of laser power and enabling fine control of the shape of the potential landscape, it has some limitations. The time-averaging requirement that the potential be painted at a rate significantly higher than the guide trapping frequency limits the trapping frequencies attainable with the current acousto-optic deflector technology to several kilohertz. While it is usually a good approximation to regard the painted potential as static, in some circumstances the time-varying phase imprinted by the painting beam can be an issue (Bell *et al.*, 2018).

3. Spatial light modulators and digital micromirror devices

A second technology for creating complex 2D potential landscapes on a light sheet relies on spatial light modulators (SLMs) that can impose amplitude or phase modulation on a laser beam that forms the desired potential after propagation through suitable optics. Two approaches have been demonstrated: a Fourier optics approach in which the SLM acts as a hologram, and a direct imaging of an intensity pattern formed by the SLM. A detailed discussion of the production of arbitrary optical potentials was presented by Gauthier *et al.* (2021). A recent demonstration for SLM realization of 3D potentials was reported by Barredo *et al.* (2018).

Early work in this direction used liquid crystal modulators to create phase holograms producing arrays of tweezer beams (Curtis, Koss, and Grier, 2002) or more complex geometries (Boyer *et al.*, 2004, 2006; Gaunt and Hadzibabic, 2012). Liquid crystal SLMs are now widely used in creating dynamic optical tweezer systems for assembling arrays of Rydberg atoms used for quantum information processing (Nogrette *et al.*, 2014). Advantages of liquid crystal modulators include the ability to impose phase or amplitude modulation on an optical beam and the possibility of using them either as holographic elements or for direct imaging, as well as a high power efficiency. The disadvantages include a limited response time for creating time-dependent potentials, as well as the technical overhead of computing real-time SLM holograms for dynamic potentials, which can be addressed using increasingly powerful graphics processing units.

An alternative to SLMs involves digital micromirror devices (DMDs) producing binary patterns over a matrix of individually switched mirrors. The intensity pattern formed by the DMD can be imaged directly onto an atomic cloud using standard imaging techniques to form intricate potentials in the image plane of the optical system. Fine intensity control overcoming the binary nature of the DMD can then be achieved through half-toning techniques (Gauthier *et al.*, 2016, 2021; Kumar *et al.*, 2016; Tajik *et al.*, 2019; Zou *et al.*, 2021). DMDs can also be used as programmable diffraction gratings, similar to SLMs, at the expenses of low power efficiency (Zupancic *et al.*, 2016). However, they offer a higher refresh rate allowing for their use in dynamical experiments (Ha *et al.*, 2015). Figure 1(b) illustrates the power of this technique for creating a BEC in the shape of a sketch of Bose and Einstein's. DMDs do suffer from flicker modulation due to their intended use in image projectors for the consumer market, so some devices may require customization for optimal use (Hueck *et al.*, 2017).

The performances of painting techniques, SLM, and DMD are summarized in the table included in Fig. 1. The three thecniques share a diffraction efficiency of $\sim 65\% - 80\%$.

B. Magnetic potentials

1. Magnetic traps

Magnetic trapping lies at the heart of many cold-atom quantum technologies. Here we sketch the logic of the technique. Magnetic traps confine spin-polarized atoms of nonzero magnetic moment to a local minimum of a static magnetic field **B**. If the magnetic field at the center-of-mass

position of an atom is sufficiently large and varies slowly, then its spin follows its change in direction and magnitude. The Zeeman energy of spin-polarized atoms ($V = -\boldsymbol{\mu} \cdot \mathbf{B}$) can then be written as $V = m_F g_F \mu_B |\mathbf{B}|$, with $m_F = \{-F, \ldots, F\}$ the magnetic hyperfine number, g_F the Landé g factor, and μ_B the Bohr magneton. Maxwell's equations forbid the generation of a dc magnetic field maximum in free space. Therefore, one has to trap so-called low-field-seeking states, whose energy increases with magnetic field strength. The field strength of the magnetic minimum has to be sufficiently large in order to prevent nonadiabatic spin-flip transitions to lower-energy (high-field-seeking) states. The latter can cause atoms to be expelled from the trap (Majorana, 1932). The two most common magnetic configurations are the Ioffe-Pritchard (IP) (Baiborodov *et al.*, 1963; Pritchard, 1983) and time-orbiting potential (TOP) (Petrich *et al.*, 1995) traps.

An IP trap consists of a radial quadrupole and an axial parabolic field, which together generate an elongated local minimum in the magnetic field. Typical values for the radial trap frequency range from few hundreds for macroscopic traps to a few thousand hertz for chip-based traps (Hänsel *et al.*, 2001). Typical axial frequencies are a few tens of hertz. Macroscopic IP traps are usually formed by a combination of large racetrack-shaped coils for the radial gradient and small "pinch" coils for the parabolic axial field. It is also possible to use structures from permanently magnetized materials, thereby allowing the creation of larger magnetic gradients and thus steeper traps. They also provide a larger degree of freedom in design compared to their purely electromagnetic counterparts, albeit at the cost of an inability to dynamically change the strength of the confinement or easily release the atoms from the trap (Tollett *et al.*, 1995; Davis, 1999; Sinclair *et al.*, 2005; Fernholz *et al.*, 2008).

The TOP trap uses a static magnetic quadrupole field, the center of which is displaced away from the atoms using a rotating magnetic homogeneous offset field (Petrich *et al.*, 1995; Hodby *et al.*, 2000). This oscillating field may be modified locally using inductively coupled conducting structures (Pritchard *et al.*, 2012; Sinuco-León *et al.*, 2014). Care must be taken for the offset field to rotate slow enough for the spin of the atoms to be able to follow, but fast enough for the center of mass of the atoms not to be significantly affected. If this condition is fulfilled, then the atoms will be trapped in the time average of the magnetic potential. For a static magnetic quadrupole field with an offset field rotating in the symmetry plane, this will result in a trap with the shape of an oblate sphere and the trapping frequencies $\omega_z = \sqrt{8}\omega_x = \sqrt{8}\omega_y$, with typical trapping frequencies from $\omega_z/2\pi = 40$ Hz to 1 kHz.

2. Atom chips

A simple atom trap can be produced by applying a transverse homogeneous magnetic field to the one produced using a single wire (Schmiedmayer, 1995a). By shaping the wires on a surface, "atom-chip" traps (Reichel, Hänsel, and Hänsch, 1999; Folman *et al.*, 2000; Hänsel *et al.*, 2001) consisting of microsized current-carrying wires can be efficiently manufactured using standard semiconductor technologies. These thin wires can be efficiently cooled through the substrate and thus permit large current densities resulting in large magnetic gradients; see Fig. 2. Consequently, trapping frequencies of 10 kHz can be achieved. Another advantage is the ability to create in 2D complex wire structures (Folman *et al.*, 2000; Fortágh and Zimmermann, 2007; Keil *et al.*, 2016). Simple H-, T-, U-, Y-, and Z-shaped wires can create a wide range of fields. For example, a magnetic IP trap can be formed using an elongated Z-shaped structure and a 3D quadrupole trap with a simple U-shaped wire (Reichel, Hänsel, and Hänsch, 1999), and a 2D quadrupole can be formed from three parallel wires, thus creating a matter-wave waveguide along which atoms can be propagated (Folman *et al.*, 2000; Long *et al.*, 2005). Cryogenically cooled atom chips have also allowed superconducting devices to be incorporated (Hyafil *et al.*, 2004; Nirrengarten *et al.*, 2006; Mukai *et al.*, 2007; Salim *et al.*, 2013). Atom chips have thus become compact hybrid platforms to trap, prepare, manipulate, and measure cold atoms. They provide the route to miniaturize and interface different atomtronic components in more complex devices (Birkl *et al.*, 2001; Gehr *et al.*, 2010; Salim *et al.*, 2013).

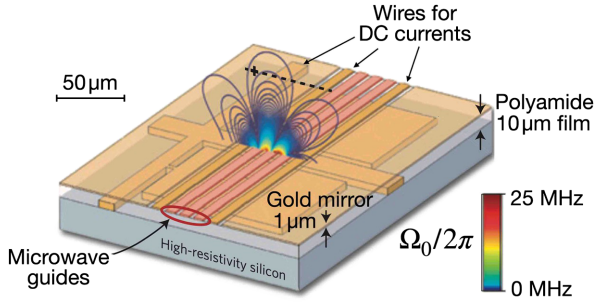

FIG. 2. Schematic drawing of an atom chip including its magnetic potentials. Atom chips can be used for double-well physics in 1D and crossover regimes, which is enabled by the ability to create robust double-well potentials using rf dressing of the atoms. Adapted from Böhi *et al.*, 2009.

Corrugation and noise currents in the conducting wires of an atom chip represent an important challenge to atom-chip-based atomtronic circuits that allow a coherent flow of atoms over macroscopic distances (Folman *et al.*, 2002; Henkel *et al.*, 2003). These noises can emerge from diverse causes ranging from current scattering due to unintended changes in the flow of direction of the current, noises in the power supplies, or magnetic impurities (Kraft *et al.*, 2002; Leanhardt *et al.*, 2002; Krüger *et al.*, 2007; David *et al.*, 2008) to thermal Johnson noise (Dikovsky *et al.*, 2005). Routes to reduce corrugations in waveguides were studied by Schumm *et al.* (2005) and Trebbia *et al.* (2007). However, the mere fact that the shape of the atom-chip potentials is defined by wire structures means that any imperfections in the wires cause defects and roughness in these potentials and make the single mode propagation over a long distance difficult to achieve.

3. Adiabatic magnetic potentials

Adiabatic magnetic potentials offer an interesting alternative to chip-based structures. They can be used to create a limited number of perfectly smooth trapping structures, such as bubbles, rings, and sheets. They occur when a radio-frequency field ($\mathbf{B}_{rf}$) strongly couples magnetic hyperfine

states and are readily described in the dressed-atom picture (Cohen-Tannoudji and Reynaud, 1977). When the radio-frequency field is resonant with the magnetic field, i.e., $\omega_{\rm rf} = \omega_{\rm L}$, the coupling strength can be expressed as the Rabi frequency $\Omega_0 = g_{\rm F}\mu_{\rm B}B_{\rm rf}^{\perp}/\hbar$, where $B_{\rm rf}^{\perp}$ is the amplitude of the circularly polarized component of $\mathbf{B}_{\rm rf}$ that is orthogonal to $\mathbf{B}$ and couples the $m_{\rm F}$ states. For an arbitrary detuning $(\delta = \omega_{\rm rf} - \omega_{\rm L})$ of the rf field from the resonance, the dressed potential can be expressed as $U(\mathbf{r}) = m'_{\rm F}\hbar\sqrt{\delta^2(\mathbf{r}) + \Omega_0^2(\mathbf{r})}$. Note that the potential is equal to the nondressed Zeeman states with $m'_{\rm F} = m_{\rm F}$ for $\delta \gg \Omega_0$, and inversely that it is equal to the nondressed Zeeman states with $m'_{\rm F} = -m_{\rm F}$ for $\delta \ll -\Omega_0$.

We now examine the simple case of a magnetic quadrupole field, where the magnitude of the field increases linearly in all directions. In any direction starting at the center and moving outward, there is some point at which the rf field becomes resonant. The dressed field therefore forms an oblate bubble-shaped trap that has a radius of $r_\rho = \hbar\omega_{\rm rf}/|g_{\rm F}|\mu_{\rm B}\alpha$ in the x-y plane and $r_{\rm z} = \hbar\omega_{\rm rf}/|g_{\rm F}|\mu_{\rm B}2\alpha$ in the z direction, where α is the quadrupole field of the gradient.

The idea was originally proposed by Zobay and Garraway (2001) and was first realized by Colombe *et al.* (2004). Thorough reviews of these traps were given by Garraway and Perrin (2016) and Perrin and Garraway (2017).

The dressed quadrupole field itself presents a problem in that any homogeneous $B_{\rm rf}$ has one or two points on the bubble where, due to the projection of the rf onto the local quadrupole field, the coupling field $B_{\rm rf}^{\perp}$ is zero, leading to Majorana spin-flip losses. This can be avoided using an IP-type trap, where the magnetic field points predominantly in the direction of the z axis. In the absence of gravity, the quantum fluid can fill the entire bubble (Sun *et al.*, 2018). These hollow Bose-Einstein condensates are currently under investigation at the International Space Station (Frye *et al.*, 2021). On Earth, however, gravity deforms the bubble trap into something more akin to a cup, which can be exploited for 2D quantum gases for its strong (weak) confinement in the vertical (horizontal) direction. Using multiple rf frequencies, multiple shells can be manipulated almost independently (Bentine *et al.*, 2017) and exploited for matter-wave interferometry (Mas *et al.*, 2019).

A dressed quadrupole trap can be used to create a matter-wave ring due simply to the angular momentum of the trapped atoms, and thus approaching a giant vortex state (Sherlock *et al.*, 2011; Guo *et al.*, 2020); see Fig. 3. Alternatively, one can combine the rf bubble trap with a red-detuned light sheet, thus forming a ring-shaped trap (Morizot *et al.*, 2006).

4. Time-averaged adiabatic potentials (TAAPs)

Highly versatile and controllable potentials in a large variety of perfectly smooth shapes can be created by combining the aforementioned adiabatic potentials with an oscillating, homogeneous magnetic field. If the Rabi frequency of the rf dressing field is large compared to the frequency of the oscillating field $\Omega_0 \gg \omega_{\rm m}$, the resulting trapping potential is the time average of the adiabatic and modulation potentials (Lesanovsky and von Klitzing, 2007; Navez *et al.*, 2016). Starting with a simple quadrupole field and adding a vertically

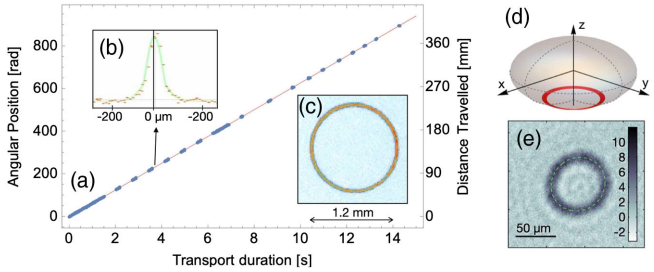

FIG. 3. (a) Long-distance transport in a ring-shaped TAAP waveguide. The angular position of the condensate and thermal cloud is shown during 14 s of transport in the matter-wave guide (blue dots) over a distance of more than 40 cm. The red line depicts the programmed trajectory of $2\pi 10$ rad s^{-1}. (b) Bimodal distribution of the BEC after 4.1 s of transport and a TOF expansion of 24 ms, with the black arrow indicating the relevant data point. See also Pandey *et al.* (2019). (c) False-color absorption image of an annular condensate in a TAAP trap. (d) Graphical illustration of atoms in a dynamically created ring trap and (e) an absorption image of a BEC in it. Adapted from Guo *et al.*, 2020.

polarized rf field, plus a vertical modulation field, one can generate a ring-shaped trap. Typical values are $50 - 100$ Hz for the radial and axial trapping frequencies and 50 μm to 1 mm for the radius. The ring can then be adiabatically turned into one or two coupled half-moon-shaped traps simply by changing the polarization of the rf or modulation fields. Multiple concentric or stacked rings can be created using more than one rf frequency.

The exact shapes of these traps and the barriers between them depend only on the amplitude and polarization of oscillating magnetic fields, which can be adjusted with extreme precision using standard electronics, making it possible to control the trapping potentials down to the picokelvin level.

Using a suitable choice of polarization, it is also possible to trap two different spin states in identical effective potentials and even to manipulate them entirely independently (Navez *et al.*, 2016). This technique might be exploited in an atom interferometer, where the atoms are placed in the TAAP in a single hyperfine state and exposed to a suitable microwave pulse. The hyperfine states of the resulting superposition can then be manipulated separately, making them sensitive to gravitation, for instance, and then recombined with a second microwave pulse (resulting in a highly sensitive interferometer) (Navez *et al.*, 2016). A similar scheme has been proposed for adiabatic ring-shaped potentials resulting from specially tailored magnetic fields (Stevenson *et al.*, 2015).

Another feature of the TAAP rings is the extreme smoothness of these potentials (Pandey *et al.*, 2019). Its shape is not determined by current-carrying structures in proximity but by a quadrupole field and the frequency and amplitude of the modulation fields, which are all generated by distant coils. Therefore, any imperfections in the field-generating coils are exponentially suppressed on the size scale of the trapping potentials; see Fig. 3. This is evidenced by Navez *et al.* (2016), where a Bose-Einstein condensate is transported at hypersonic speeds for a distance of 15 cm without loss in spatial coherence.

C. Atom optical elements

In this section, we outline the types of potentials and the optical elements that have been designed to guide the matter waves in atomtronic circuits.

1. Waveguides

The fabrication of one-dimensional guides is important in an atomtronic context, both to control the circuit functionalities and to explore quantum effects in fundamental physics. The coherent regime needs to consider both the tightness of the confinement and any displacement or roughness of the waveguide transverse to the direction of propagation. Operating in the strict one-dimensional regime requires the transverse frequencies to be much larger that both the chemical potential and the temperature of the gas, as well as the kinetic energy originating from the current flowing in the system. This can be achieved using tight optical confinement from optical lattices (Bloch, Dalibard, and Zwerger, 2008) or projected wires (Krinner, Esslinger, and Brantut, 2017). Optical lattices with a typical lattice spacing of a few microns have been realized (Rubinsztein-Dunlop *et al.*, 2017). In such structures, in which the cold atoms can tunnel between the lowest Bloch bands of the adjacent wells, the low temperature matter-wave effective dynamics is one dimensional.

A rapid modulation of the strength of the transverse confinement or a bend in the waveguide couples the forward motion of the atoms to oscillations of the condensate via its chemical potential. It also causes a shift of the potential energy of the bottom of the waveguide, which can induce scattering, although it is possible to shape a slow bend to avoid this effect (del Campo, Boshier, and Saxena, 2014). As pointed out in Sec. II.B.2, this regime is difficult to achieve with atom chips. Excitationless matter-wave guides have been demonstrated using single-beam optical dipole beams over distances of 3.5 mm (McDonald, Keal *et al.*, 2013) and using TAAPs over distances of 40 cm for thermal clouds and 15 cm for BECs (Pandey *et al.*, 2019). Waveguide bends and junctions created with painted potentials have demonstrated excitation probabilities of less than 8% (Ryu and Boshier, 2015).

The requirements for precision interferometers are rather stringent. Care must be taken to ensure that the superposition state traverses the interferometer adiabatically and that the trap-induced energy difference between the two paths is extremely well controlled (Kreutzmann *et al.*, 2004; Zabow, Conroy, and Prentiss, 2004). For propagating matter-wave interferometers, this results in extreme requirements on corrugations of the waveguides since any small lateral deviation tends to couple the forward motion to transverse modes (thus destroying the coherence of the superposition state). In the absence of such coupling the interferometer are expected to be able to operate using multiple transverse modes concurrently (Andersson *et al.*, 2002).

2. Ring traps

Ring traps are the simplest spatially closed atomtronic circuits. They normally consist of a tight harmonic confinement in the vertical and horizontal directions and no confinement along the azimuthal direction. The potential for a ring of radius ρ_0 can be written near the trap minimum as $U = (1/2)m\omega_\rho^2(\rho - \rho_0)^2 + (1/2)m\omega_z^2 z^2$, with m the mass of the atoms and ω_ρ and ω_z the harmonic trapping frequencies in the radial and vertical directions, respectively. There are two distinct regimes of interest in ring traps: One where the radius of the ring is small enough for the energy or timescale of the excitations along the circumference of the ring to become important, and one where the ring is to be viewed more like a circular waveguide.

Early demonstrations focused on atom propagation in large ring-shaped waveguides. Large-scale magnetic traps have been demonstrated in which the shape of the ring is directly defined by the field-generating wires using either microfabricated atom chips (Sauer, Barrett, and Chapman, 2001) or large wire structures (Gupta *et al.*, 2005; Arnold, Garvie, and Riis, 2006) and inductively coupled rings (Pritchard *et al.*, 2012). For polar molecules electrostatic ring traps have also been demonstrated (Crompvoets *et al.*, 2001).

Small-diameter ring traps can be generated using purely optical dipole potentials. The first toroidal BEC was created using a painted potential (Henderson *et al.*, 2009). Static approaches to creating rings with optical potentials include the use of a light sheet in combination with a Laguerre-Gauss beam (Wright, Arlt, and Dholakia, 2000; Ramanathan *et al.*, 2011; Moulder *et al.*, 2012). Persistent currents in spinor condensates were detected by Beattie *et al.* (2013). In this case, the imperfections in the potential often do not lead to adverse effects since the superfluid nature of the flow smooths them over. Examples include studies of supercurrents (Moulder *et al.*, 2012; Eckel, Lee *et al.*, 2014; Ryu, Henderson, and Boshier, 2014) and Josephson junctions (Ryu *et al.*, 2013; Wright *et al.*, 2013a).

Optical ring lattices suitable for trapping cold and quantum degenerate atomic samples have been generated with Laguerre-Gauss laser beams incident on SLM or manipulated by an acousto-optical modulator (Franke-Arnold *et al.*, 2007; Henderson *et al.*, 2009; Amico *et al.*, 2014). By applying computer assisted optimization algorithms using absorption images of BECs in the dipole potentials, smooth potentials of ring radii and lattice spacings of 100 and 30 μm, respectively, have been demonstrated. DMD generated rings lattices of $\sim$40 μm and lattice spacing of $\sim$4 μm have been achieved (Gauthier *et al.*, 2016). However, to achieve any appreciable tunneling among the lattice wells, these numbers need to be further scaled down.

Finally, ultrasmooth ring-shaped waveguides based on TAAPs (Lesanovsky and von Klitzing, 2007) have recently been demonstrated. They support a coherent, lossless transport of matter waves over macroscopic distances (14 cm) even at hypersonic speeds (Pandey *et al.*, 2019).

3. Barriers and beam splitters

The terms "barrier" and "beam splitters" are distinguished primarily by their intended use rather than the underlying function or principles. To borrow a term from optics, beam splitters are familiar elements, particularly in the context of interferometers, used for coupling a pair of system modes. Barriers are commonly used to define spatially distinct regions

having different potential structures, temperatures, and chemical potentials, as is the case in triple-well transistors (Caliga *et al.*, 2016). Beam splitters have been implemented using both time-dependent and time-independent potentials, whereas barriers are typically implemented with time-independent potentials.

Early work on atomtronic beam splitters split magnetically guided thermal atoms utilizing Y- or X-shaped conductor junctions, resulting in multimode splitting (Cassettari *et al.*, 2000; Müller, Cornell, Prevedelli *et al.*, 2000). Coherent beam splitting on an atom chip has been carried out using Bragg diffraction from an optical lattice that is exposed to the atoms in a double-pulsed manner (Diot *et al.*, 2004; Wang *et al.*, 2005). Coherent splitting of stationary Bose condensates produced on atom chips has also been carried out utilizing radio-frequency fields that provide an elegant means of evolving in time a single magnetically generated potential well into a double well, and vice versa (Schumm *et al.*, 2005; Hofferberth *et al.*, 2006; Kim *et al.*, 2017). Note that earlier successes in coherent beam splitting utilized time-dependent potentials.

In the framework of atomtronic circuitry there is a particular interest in beam splitters that are spatially fixed and time independent. The use of painted potentials (Henderson *et al.*, 2009) enabled coherent splitting of a propagating condensate in Y junction optical waveguides (Ryu and Boshier, 2015), while beam splitting in crossing optical waveguides has also been carried out using an optical Bragg grating produced by a pair of interfering laser beams located at the waveguide junction (Guarrera *et al.*, 2017).

In contrast to the coherent splitting that is achieved with waveguides coupled by spatial proximity or through optical gratings, barriers act more like the mirrors and beam splitters of optical systems. Barriers produced using projected blue-detuned laser beams feature a smooth Gaussian profile. Coherent splitting occurs due to tunneling and quantum reflection for atoms with energies below or above the top of the barrier, respectively, within an energy range proportional to the inverse curvature of the barrier at its top (Cuevas and Scheer, 2017). Matter-wave propagation across arbitrary arrangements of barriers can be numerically calculated utilizing the impedance method (Khondker, Khan, and Anwar, 1988; Gutiérrez-Medina, 2013), a technique that borrows wave propagation techniques from electromagnetic transmission line analysis.

Projected optical atomic potentials that affect the center-of-mass motion through ac Stark shifts are limited in size scale by the wavelength of the projected light. Barriers having sub-wavelength size scales down to less than 50 nm have been demonstrated using the nonlinear response of the dark state of a three-level system (Lacki *et al.*, 2016; Wang *et al.*, 2018).

Regarding the large variety of approaches in barrier and beam splitter implementation, it is not evident that a single approach has emerged as the one best suited for atomtronic systems. Rather, the optimum approach is purpose dependent. What has emerged, however, is that it has proved to be difficult to achieve coherence-preserving barriers or beam splitters using purely magnetic approaches. Either all optical or hybrid magnetic and optical or radio-frequency systems have met with good success.

III. COHERENT EFFECTS IN MESOSCOPIC MATTER-WAVE CIRCUITS

Like their electronic counterparts (Cuevas and Scheer, 2017), atomtronic devices can operate in a regime where quantum interference plays a dominant role. Such a coherent regime is achieved in situations where the typical transport scale, such as the circumference of a ring trap or the length of a mesoscopic section, is larger than the typical decay length of the particles' correlation function. Phenomena such as Aharonov-Bohm interference, Bragg reflection on periodic structures, and Anderson localization emerge in the transport properties. Quantum-coherent transport is deduced from properties of the Hamiltonian describing the atoms inside the conductor that are identical to the coherent wave propagation in complex media encountered in electromagnetism.

Operating in this regime typically requires low enough temperatures: for Fermi gases, the relevant length scale is $\hbar v_F/k_B T$, where v_F is the Fermi velocity and for thermal gases the scale is the thermal de Broglie wavelength. For bosons, the emergence of the condensate below the critical temperature ensures coherence at arbitrarily large distances, making them particularly well suited for the study of coherent transport. The long wavelength dynamics is then efficiently described using superfluid hydrodynamics; see Sec. III.A.1. Many-body fermionic particles are discussed in Sec. III.A.2. Coherence properties are also affected by many-body effects such as the decrease of quasiparticle lifetime and quantum fluctuations. Furthermore, coherence can be reduced by noise, spontaneous emission from lasers, or other external disturbances.

In this section, we bridge microscopic models to simple matter-wave circuits. The various model Hamiltonians describing coherent quantum fluids with different features are introduced. We then focus on the persistent current in ring-shaped circuits providing both an important figure of merit for the system's coherence and an elementary building block for atomtronic circuits. Finally, we present the two-terminal quantum transport and illustrate the specific features emerging from the coherent quantum dynamics.

A. Model Hamiltonians

The many-body Hamiltonian describing N interacting quantum particles of mass m subjected to an effective magnetic field described by the vector potential $\mathbf{A}$ and confined in the potential V_{ext} reads

$$H = \int d\mathbf{r}\Psi^\dagger(\mathbf{r})\left[\frac{1}{2m}[-i\hbar\boldsymbol{\nabla} + \mathbf{A}(\mathbf{r})]^2 + V_{\text{ext}}(\mathbf{r})\right]\Psi(\mathbf{r}) + \frac{1}{2}\int d\mathbf{r}d\mathbf{r}'\Psi^\dagger(\mathbf{r})\Psi^\dagger(\mathbf{r}')v(\mathbf{r}-\mathbf{r}')\Psi(\mathbf{r})\Psi(\mathbf{r}'), \quad (1)$$

where $\Psi^\dagger(\mathbf{r})$ and $\Psi(\mathbf{r})$ are field operators creating or annihilating a bosonic or fermionic particle at the spatial position $\mathbf{r}$ (Mahan, 2013) and $v(\mathbf{r}-\mathbf{r}')$ is the two-body interparticle interaction. We assume contact interactions $v(\mathbf{r}-\mathbf{r}') = g\delta(\mathbf{r}-\mathbf{r}')$, with $g = 4\pi\hbar^2 a_s/m$ and a_s the s-wave scattering length. $\mathbf{A}$ is an effective gauge potential, which plays a crucial

role in the description of currents in spatially closed geometries. Both lattice and continuous systems are relevant for atomtronic circuits. The quantum many-body theories are presented mostly for the one-dimensional case. They are used to describe quantitatively tightly confined geometries, such as quantum wires and point contacts, but also qualitatively capture the physics of extended systems along the transport direction. Given their relevance for specific atomtronic circuits, the Gross-Pitaevskii mean-field theories are also discussed for higher dimensions.

1. Bosons

In this case the field operators obey the commutation relations $[\Psi(\mathbf{r}),\Psi^\dagger(\mathbf{r}')]=\delta(\mathbf{r}-\mathbf{r}')$. For a recent review on one-dimensional bosons, see Cazalilla *et al.* (2011). We start with a lattice theory describing atoms localized in potential wells centered in N_s sites and expand the field operators in Wannier functions, which are assumed to be a good basis of eigenfunctions of separated local potential wells: $\Psi(\mathbf{r})=\sum_{j=1}^{N_s} w(\mathbf{r}-\mathbf{r_j})a_j$, in which the operators $\hat{a}_j$ create a single bosonic particle at the site j, $[a_i,a_j^\dagger]=\delta_{ij}$. Using the previous expression of $\Psi(\mathbf{r})$, the many-body Hamiltonian can be recast to the Bose-Hubbard model (BHM),

$$\mathcal{H}_{\mathrm{BH}}=\sum_{\langle i,j\rangle}^{N_s}\left[-J(a_ja_{j+1}+a_{j+1}a_j)+\frac{U}{2}n_j(n_j-1)\right], \quad (2)$$

in which we assume that only atoms in nearest neighbor local wells can appreciably overlap. A ring geometry is assumed such that $a_{N_s+1}^\dagger=a_1^\dagger$. The parameters in the Hamiltonian are the hopping amplitude $J=\int d\mathbf{r}w^*(\mathbf{r}-\mathbf{r}_i)\{(1/2m)[-i\hbar\boldsymbol{\nabla}+\mathbf{A}(\mathbf{r})]^2+V_{\mathrm{ext}}\}w(\mathbf{r}-\mathbf{r}_{i+1})$ and the interaction strength $U=\pi a_s\int d\mathbf{r}|w(\mathbf{r})|^4/m$. The Hamiltonian (2), originally introduced as a lattice regularization of the continuous theory of bosonic fields (Haldane, 1980), provides a paradigmatic model to study Mott insulator–superfluid quantum phase transitions (Fisher *et al.*, 1989). The BHM is extensively used in mesoscopic physics (Fazio and Van Der Zant, 2001). The conditions for the realization of the BHM in cold-atom systems were identified by Jaksch *et al.* (1998), and since then it has provided an important scheme in the cold-atom quantum technology (Bloch, Dalibard, and Zwerger, 2008). For neutral matter, the vector potential $\mathbf{A}(\mathbf{x},t)$ provides an artificial gauge field (Dalibard *et al.*, 2011; Goldman *et al.*, 2014); see Sec. III.B.1. For sufficiently smooth $\mathbf{A}(\mathbf{x},t)$ on the atomic scale, the gauge field can be absorbed into the Wannier functions $\tilde{w}(\mathbf{r}-\mathbf{r}_i)=e^{-i\Lambda(\mathbf{r},t)}w(\mathbf{r}-\mathbf{r}_i)\approx e^{i\Lambda(\mathbf{r}_i,t)}w(\mathbf{r}-\mathbf{r}_i)$, with $\Lambda(\mathbf{r},t)=\int_{\mathbf{r}_0}^{\mathbf{r}}\mathbf{A}(\mathbf{r},t)d\mathbf{r}$, where $\mathbf{r}_0$ is an arbitrary lattice site. Therefore, the hopping parameter results in $J=e^{i\Phi}J_0$ and $\Phi=\int_{\mathbf{r}_i}^{\mathbf{r}_{i+1}}\mathbf{A}(\mathbf{r},t)d\mathbf{r}$. The procedure of absorbing the effects of the gauge field into the hopping matrix element is called Peierls substitution (Peierls, 1933; Essler *et al.*, 2005).

In the limit of a large average number of particles per site $\nu=N/N_s\gg 1$, the Bose-Hubbard Hamiltonian effectively reduces to the quantum phase model (QPM) (Fazio and Van Der Zant, 2001) as follows:

$$\mathcal{H}_{\mathrm{QP}}=-2J_{\mathrm{E}}\sum_{\langle i,j\rangle}^{N_s}\left[\cos(\hat{\phi}_i-\hat{\phi}_j-\Phi)+\frac{U}{2}\sum_{j=1}^{N_s}\hat{Q}_j^2\right], \quad (3)$$

where $J_{\mathrm{E}}=JN_{\mathrm{s}}$, $\hat{Q}_j=n_j-N/N_{\mathrm{s}}$ are the on-site particle-number fluctuations, and ϕ_j are the Hermitian phase operators (Amico, 2000; Amico and Penna, 2000). The operators satisfy the commutation relations $[\hat{\phi}_i,\hat{Q}_j]=i\hbar\delta_{ij}$.

In the limit of small filling fractions $\nu=N/N_s\ll 1$, the lattice Hamiltonian (2) leads to the Bose-gas continuous theory. This statement holds true since the filling is proportional to the lattice spacing Δ: $\nu=D\Delta$, with D the particle density. To have a well-defined result in the continuous limit $\Delta\to 0$, the bosonic operators must be rescaled: $\hat{a}_i=\sqrt{\Delta}\Psi(\mathbf{r}_i)$, $\hat{n}_i=\Delta\Psi^\dagger(\mathbf{r}_i)\Psi(\mathbf{r}_i)$, and $\mathbf{r}_i=\mathbf{i}\Delta$. The BHM reads (Korepin, Bogoliubov, and Izergin, 1997) $H_{\mathrm{BH}}=t\Delta^2\mathcal{H}_{\mathrm{BG}}$ and $\mathcal{H}_{\mathrm{BG}}=\int d\mathbf{r}[(\partial_{\mathbf{r}}\Psi^\dagger)(\partial_{\mathbf{r}}\Psi)+c\Psi^\dagger\Psi^\dagger\Psi\Psi]$, with $c=U/t\Delta$ (Amico and Korepin, 2004). This coincides with Eq. (1), where $c=mg/\hbar^2$. We note that, while the procedure is valid for any U, the attractive case demands smaller values of Δ for the actual mapping of the spectrum (Oelkers and Links, 2007). This feature is due to formation of a quantum analog of bright solitons (Naldesi *et al.*, 2019).

The many-body Hamiltonian arising from $\mathcal{H}_{\mathrm{BG}}$ in first quantization is known as the Lieb-Liniger model and reads

$$\mathcal{H}_{\mathrm{LL}}=\sum_{j=1}^{N_p}\frac{\hbar^2}{2m}\left(-i\frac{\partial}{\partial x_j}-\frac{\Phi}{2\pi N_s}\right)^2+g\sum_{1\le j<k<N_p}\delta(x_j-x_k). \quad (4)$$

We note that even though the Bose-Hubbard model is not integrable (Choy and Haldane, 1982; Amico and Korepin, 2004; Dutta *et al.*, 2015), the 1D Bose gas is, with the exact solution given by Lieb and Liniger using the Bethe ansatz (Lieb and Liniger, 1963).

With a fully factorized (not-entangled) ansatz for the many-body wave function $\Psi_{\mathrm{GS}}(\mathbf{r}_1,\ldots,\mathbf{r}_N)=(1/N)\prod_j^N\phi(\mathbf{r}_j)$, the dynamics entailed by the Hamiltonian (1) reduces to the following Gross-Pitaevskii equation (Calogero and Degasperis, 1975; Dalfovo *et al.*, 1999; Leggett, 2006):

$$i\hbar\partial_t\phi(\mathbf{r},t)=\left[\frac{\hbar^2}{2m}(-i\boldsymbol{\nabla}-\mathbf{A})^2+V_{\mathrm{ext}}(\mathbf{r})+gN|\phi(\mathbf{r})|^2\right]\phi(\mathbf{r}), \quad (5)$$

in which we restored the 3D character of the system since many relevant applications of the Gross-Pitaevskii equation (GPE) occur in circuits of higher dimensionality (such as toroidal confinements). We note that $\sqrt{N}\phi(\mathbf{r})$ coincides with $\langle\Psi(\mathbf{r},t)\rangle$, which is defined by the mean-field approximation of the Heisenberg equations of the motion stemming from the Hamiltonian (1). The reduction of the quantum many-body problem to the GPE dynamics is well justified in the dilute regime, i.e., when $a_s^3\rho\ll 1$; see Lee, Huang, and Yang (1957) for corrections. In one dimension, taking $A=0$ and $V_{\mathrm{ext}}=0$ the Gross-Pitaevskii equation is integrable with solitonic solutions (Faddeev and Takhtajan, 2007). Equation (5), recast in amplitude phase representation $\phi=\sqrt{n}e^{i\theta}$, gives rise to the

superfluid hydrodynamics equations for the condensate density n and the phase θ (Dalfovo *et al.*, 1999).

2. Fermions

Here we refer to a gas of fermions with κ components or colors. In this case, the field operators are characterized by the spin label $\alpha = \{1, \ldots, \kappa\}$. They obey the following anticommutation rules: $\{\Psi_\alpha(\mathbf{r}), \Psi^\dagger_{\alpha'}(\mathbf{r}')\} = \delta_{\alpha,\alpha'}\delta(\mathbf{r}-\mathbf{r}')$. By employing a derivation similar to that previously described for the bosonic case, one can obtain the generalization of the Hubbard model. If the physical parameters of the system, like interaction or trapping potentials, turn out to be independent by the color, then the κ component fermions are known as SU(κ) fermions. The Hamiltonian for SU(κ) fermions in a ring lattice pierced by an effective gauge field reads (Capponi, Lecheminant, and Totsuka, 2016)

$$\mathcal{H}_{\mathrm{SU}(\kappa)} = -J\sum_{j=1}^{N_s}\sum_{\alpha=1}^{\kappa}(e^{i\Phi}c^\dagger_{\alpha,j}c_{\alpha,j+1} + \mathrm{H.c.}) + U\sum_{\alpha\neq\alpha' j} n_{\alpha,j}n_{\alpha',j}, \tag{6}$$

where $c^\dagger_{\alpha,j}$ creates a fermion at the site j of a d-dimensional lattice with a spin component α, $n_{\alpha,j} = c^\dagger_{\alpha,j}c_{\alpha,j}$ is the local number operator for site j and spin component α. The parameters J and U account for the hopping strength and on-site interaction, respectively. They can be expressed in terms of the integrals of the Wannier functions as discussed for the bosonic case. For $\kappa = 2$, this provides a paradigmatic framework to address the physics of itinerant electrons in a d-dimensional lattice (Gutzwiller, 1963; Hubbard, 1963; Kanamori, 1963). See Baeriswyl *et al.* (2013), Mahan (2013), and Mielke (2015) for more recent discussions. Systems of two spin components (Jördens *et al.*, 2008), and more recently of κ-component fermions (Cappellini *et al.*, 2014; Pagano *et al.*, 2015), have been experimentally realized with cold-atom quantum technology. For $\kappa = 2$, the Hamiltonian (6) is integrable using a Bethe ansatz for any values of system parameters and filling fractions $\nu = N/L$ (Lieb and Wu, 1968). For $\kappa > 2$, the Bethe ansatz integrability is preserved in the continuous limit of vanishing lattice spacing, with Eq. (6) turning into the Gaudin-Yang-Sutherland model describing SU(κ) fermions with a delta interaction (Sutherland, 1968). This regime is achieved using Eq. (6) in the dilute limit of small filling fractions. Bethe ansatz solutions allow a precise understanding of both the ground state and the nature of excitations of the system. The corresponding Hamiltonian reads

$$H_{\mathrm{GYS}} = \sum_{\alpha=1}^{\kappa}\sum_{j=1}^{N}\frac{\hbar^2}{2m}\left(-i\partial_{x_{j,\alpha}} - \frac{\Phi}{2\pi N_s}\right)^2 + g\sum_{1\le i<j\le N}\sum_{\alpha,\beta=1}^{\kappa}\delta(x_{i,\beta}-x_{j,\alpha}). \tag{7}$$

Another integrable regime of Sec. III.A.2 is obtained for $\langle\sum_\alpha n_{\alpha,j}\rangle = 1 \ \forall \ j$ and large repulsive values of $U \gg t$ for which the system is governed by the SU(κ) antiferromagnetic Sutherland model (Sutherland, 1975; Guan, Batchelor, and Lee, 2013; Capponi, Lecheminant, and Totsuka, 2016). In the intermediate interactions and intermediate fillings, the model in Sec. III.A.2 for $\kappa > 2$ is not integrable and approximated methods are needed to access its spectrum. SU(2) and SU(κ) fermions benefit from a different physics. For spin 1/2 fermions, spin excitations, the so-called spinons, are gapless in the thermodynamic limit; charge excitations are instead gapped at half filling (the Mott phase) and gapless otherwise (Andrei, 1995). In the low-energy limit, spin and charge excitations are separate from each other. The Mott phase is suppressed only exponentially for $\kappa = 2$ (Lieb and Wu, 1968). For $\kappa > 2$, fermions display a Mott transition for a finite value of U/J (Manmana *et al.*, 2011; Cazalilla and Rey, 2014). For incommensurate fillings, a superfluid behavior is found. In the SU(κ) case, the spin and charge excitations can be coupled (Affleck, 1988).

3. Impurities, weak links, and contacts

Barriers, weak links, quantum impurities, and contacts are essential features for matter-wave circuits. Most, if not all, of these features can be experimentally realized, with a wide range of parameters in both the spatial and time domains. We now sketch how they can be incorporated in the systems Hamiltonian.

In continuous systems [like Eqs. (4), (5), and (7)], ideal localized barriers can be modeled as delta-function potentials. They can be used to stir ring-shaped condensates (Hallwood, Burnett, and Dunningham, 2007; Hallwood, Ernst, and Brand, 2010; Nunnenkamp, Rey, and Burnett, 2011; Schenke, Minguzzi, and Hekking, 2011). In numerical simulations closely describing the experimental conditions, the delta function is replaced by a suitably peaked Gaussian function (Nunnenkamp, Rey, and Burnett, 2011). Localized barriers in lattice systems are achieved through weak links in the hopping amplitudes (Amico *et al.*, 2014; Aghamalyan *et al.*, 2016) or using suitable offsets of the local potentials (Aghamalyan *et al.*, 2015; Cominotti *et al.*, 2015).

In a typical transport setup, the effect of a thin localized barrier of large strength can be described using the tunnel Hamiltonian $\mathcal{H} = \mathcal{H}_L + \mathcal{H}_R + \mathcal{H}_t$, in which $\mathcal{H}_L$ and $\mathcal{H}_R$ are the left and right leads and $\mathcal{H}_t$ is the tunneling Hamiltonian. A standard expression for $\mathcal{H}_t$ is $H_t = \mathcal{J}(\psi^\dagger_L\psi_R + \mathrm{H.c.})$, where ψ_L and ψ_R are single-particle operators of the left and right leads, respectively [see Nazarov and Blanter (2009)] and $\mathcal{J}$ is the tunnel amplitude. On a semiclassical level, the two lead transports can be described in terms of the atom transfer among the reservoirs $\Delta N = N_L - N_R$. Specifically, the current is defined as $I = -(1/2)d(\Delta N)/dt$. This logic is applied in the two-terminal transport setups discussed in Sec. III.C.

B. Persistent currents in atomtronic circuits

Even though persistent currents are mesoscopic in nature, they are instrumental for atomtronics. They can provide an important tool for quantum simulation since they can probe quantum phases of matter. At the same time, persistent currents can be used for atomtronic devices such as quantum

sensing (see Sec. IV.E) and neutral current–based platforms for qubit implementations (see Sec. IV.D).

1. The concept of persistent current

The persistent current is one of the defining notions of mesoscopic physics (Büttiker, Imry, and Landauer, 1983; Imry and Landauer, 1999; Imry, 2002): in an electronic ring-shaped gas (such as a metal) pierced by a static magnetic field, a dissipationless current can occur. This is a manifestation of the electron phase coherence all along the ring, implying that the coherence length is larger than the system size. This counterintuitive phenomenon occurs in the quantum regime, where resistive effects due to interactions, the presence of impurities, and thermal fluctuations leading to decoherence are negligible. Persistent currents in electronic systems have been thoroughly studied both theoretically and experimentally [see Zvyagin and Krive (1995), Saminadayar, Bauerle, and Mailly (2004) and references therein] with the aim of shedding light on their own mechanisms, studying the effect of interactions, and understanding the role of impurities (Riedel and von Oppen, 1993; Chakraborty and Pietiläinen, 1994; Imry, 2002; Matveev, Larkin, and Glazman, 2002).

In superconductors and superfluids, the persistent currents coincide with the supercurrents flowing across the ring and originate from the macroscopic phase coherence of such quantum states. Experimental observations of persistent currents have been reported in multiple condensed-matter systems: normal metallic rings (Lévy *et al.*, 1990; Mohanty, 1999; Bleszynski-Jayich *et al.*, 2009) and superconductors (Deaver and Fairbank, 1961). Exciton polaritons have also been proposed as a platform to study persistent currents under controllable conditions (Sanvitto *et al.*, 2010; Li *et al.*, 2015; Gallemí *et al.*, 2018; Lukoshkin *et al.*, 2018).

By virtue of the control and flexibility of their operating conditions and the possibility of dealing with different particle statistics, ultracold atoms provide an ideal platform for studying persistent currents with a new scope. The study of persistent currents was initiated in cold-atom systems confined to ring-shaped potentials and pierced by a synthetic magnetic field by Amico, Osterloh, and Cataliotti (2005). Indeed, a quantum gas in ring-shaped confinement and subjected to an artificial gauge field with flux Φ (see Sec. III.A) behaves as a charged particle subjected to a magnetic field. The artificial magnetic field can be engineered using a variety of techniques in quantum technology ranging from a simple rotation to the transfer of angular momentum through two-photon Raman transitions or Berry phases and hologram phase imprinting techniques (Dalibard *et al.*, 2011; Goldman *et al.*, 2014). The effective magnetic field imparts a phase gradient on the particles' wave function that defines a finite velocity field along the ring. For sufficiently smooth guides (i.e., the most common situation in cold-atom experiments) the particles' flow is dissipationless. The current is obtained from the free energy thanks to a thermodynamic identity deduced from the Hellmann-Feynman theorem $I = -(1/2\pi)\partial F/\partial\Phi$ (Zvyagin and Krive, 1995). In the ground state, the persistent current is $I = -(1/2\pi)\partial E_{\mathrm{GS}}/\partial\Phi$.

In the quantum-coherent regime, the particle current is predicted to be a periodic function of the applied flux $\Phi = \omega R^2$ of the artificial gauge field, with R the ring radius. A theorem originally attributed to Leggett (1991) shows that, for spinless fermions and bosons with repulsive interactions on a clean ring, the persistent currents do not depend on the interaction strength but merely reflect angular momentum conservation along the ring, so the ground-state energy is written as $E = E_0(\ell - \Phi/\Phi_0)^2$, with ℓ denoting the z angular momentum quantum number; i.e., the ground-state energy is piecewise parabolic and each parabola indicates a different value of angular momentum carried by the circulating particles. The period of oscillation of the currents is the flux quantum $\Phi_0 = \hbar/m$. Inclusion of localized impurities or of a barrier mixes the angular momentum states, thus smoothing the amplitude of the persistent currents (Hekking and Glazman, 1997; Matveev, Larkin, and Glazman, 2002; Cominotti *et al.*, 2014). Such an impurity is felt by the interacting fluid as an effective localized barrier affecting the system in a way that depends on interaction. For repulsive interactions, the Luttinger liquid paradigm (Giamarchi, 2003) holds at intermediate and strong interactions and the effective barrier depends on a power law with the ring size, while for the weak interactions the barrier is screened by healing length effects (Cominotti *et al.*, 2014). The regime where the barrier effectively splits the ring into two disconnected parts is a universal function of the barrier and interaction strength (Aghamalyan *et al.*, 2015). For attractive interactions, the excitation spectrum is quadratic and a universal scaling with a nontrivial interplay of the barrier and interaction strength is observed in some interaction regimes (Polo *et al.*, 2022).

Relying on the enhanced capabilities of DMDs or painting techniques, one can engineer persistent currents using machine learning assisted dynamics of the trapping potential (Haug *et al.*, 2021). Specifically, the engineering can be achieved by training a deep-learning network on the local potential offsets, thereby trapping the atoms in a ring-shaped circuit with lumped parameters [Eqs. (2) and (3)]. This approach predicts that better performance in the state preparation and in the nature of persistent currents (currents involving three angular momenta can be engineered) can be achieved than with the existing protocols based on stirring protocols.

Persistent currents have been also studied in bosonic ring ladders (Aghamalyan, Amico, and Kwek, 2013; Polo *et al.*, 2016; Richaud and Penna, 2017; Haug, Amico *et al.*, 2018; Victorin *et al.*, 2019). Discrete vortex structures can occur there in the transverse direction, giving rise to a wealth of phases; see Amico *et al.* (2021) for a review. Josephson oscillations and orbital angular momentum dynamics in two coupled rings in a stuck configuration were studied by Lesanovsky and von Klitzing (2007), Oliinyk, Yakimenko, and Malomed (2019), and Nicolau *et al.* (2020). In multicomponent mixtures, the criterion of stability of persistent current and the relation with entanglement were addressed by Anoshkin, Wu, and Zaremba (2013), Abad *et al.* (2014), and Spehner, Morales-Molina, and Reyes (2021). The transfer of angular momentum between different bosonic species was theoretically addressed by Penna and Richaud (2017).

We close this section by summarizing the important results based on Gross-Pitaevskii dynamics in two or three spatial dimensions. In most of the protocols studied thus far, the

matter-wave flow is obtained by stirring. Many sources of decay of persistent currents have been identified: the generation of elementary excitations, thermal fluctuations, vortices, and vortex rings (Piazza, Collins, and Smerzi, 2009; Mathey, Clark, and Mathey, 2014; Wang *et al.*, 2015; Abad, 2016; Xhani *et al.*, 2020). For a tightly confined toroidal-shaped condensate, persistent currents may still decay using phase slippage mechanisms, particularly through incoherent or coherent phase slips depending on interaction and temperature regimes (Danshita and Polkovnikov, 2012; Kunimi and Danshita, 2017; Polo *et al.*, 2019). Using this approach, stirring the matter wave is studied in racetrack atomtronic circuits (Eller *et al.*, 2020).

2. Experimental observation and readout of persistent currents in bosonic toroidal-shaped atomtronic circuits

Rotating fluids and persistent currents are observed in ultracold atomic gases on a ring in a doughnut-shaped ring trap (Ramanathan *et al.*, 2011; Moulder *et al.*, 2012; Wright *et al.*, 2013a; Ryu, Henderson, and Boshier, 2014); see Figs. 4(a) and 4(b). A challenge in rotating a quantum fluid is the generation of excitations and vortices (Dubessy *et al.*, 2012; Arabahmadi, Schumayer, and Hutchinson, 2021). The threshold for creation of excitations has been measured (Wright *et al.*, 2013b). The decay of persistent currents due to thermal fluctuations has been also experimentally studied (Kumar *et al.*, 2017). Recent experiments have achieved high rotation quantum numbers, with a rotation speed of up to 18 times the sound velocity (Pandey *et al.*, 2019; Guo *et al.*, 2020).

The transition from superfluid to resistive flow is studied by introducing two moving weak links on the ring in opposite directions (Jendrzejewski *et al.*, 2014). This experiment provides a new technique: the use of a ring to address mesoscopic transport properties; see also Sec. III.C. Along the same lines, it has been demonstrated that it is possible to study the current-phase relation of a superfluid using a ring geometry (Eckel, Jendrzejewski *et al.*, 2014).

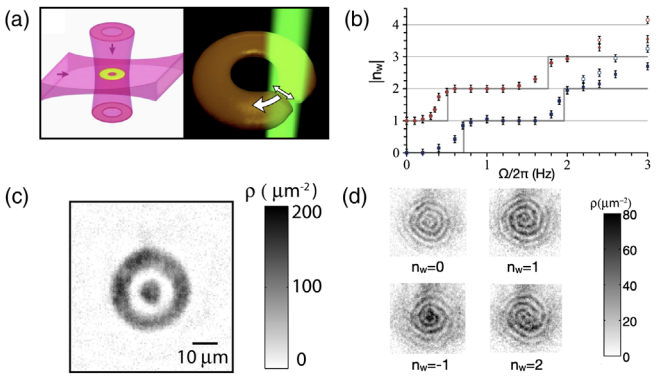

FIG. 4. Experimental realization of a BEC rotating in a circular atomtronic circuit. (a) Schematics of the fabrication of the optical potential and the stirring protocol. The circular confinement is realized through a Laguerre-Gauss laser field, the transverse confinement is implemented through light sheets, and the condensate is stirred with a rotating blue-detuned focused laser beam. (b) Persistent currents featuring quantized steps of the angular momentum imparted to the BEC expressed by the winding number n_w. (c) CCD-contrast image of a ring-shaped rotating BEC concentric with a second BEC. (d) Such a configuration allows one to probe the direction and strength of the angular momentum through characteristic spiral interferograms. (a),(b) Adapted from Wright *et al.*, 2013a. (c),(d) Adapted from Corman *et al.*, 2014.

Persistent currents can be explained with the various branches of the energy dispersion relation as a function of the flux or the rotation rate. Eckel, Lee *et al.* (2014) observed hysteresis among different branches and proposed it as a method for controlling an atomtronic device.

Readout of the currents in ultracold atomic systems can be done in various ways. The CCD-contrast image of the atom density after a long time release of the condensate from the trap is called the time of flight (TOF). In most of the experiments, the TOF image is achieved after a 10–20 ms releasing time. The theoretical approach to the TOF amounts to computing the momentum distribution of the system at the instant of time in which the trap is open ($t = 0$) (Read and Cooper, 2003). For a condensate flowing along ring-shaped circuits, the TOF displays a characteristic shape in which the density around $\mathbf{k}$ is suppressed. The TOF image (taken from the top of the expanding condensate in the falling direction) shows a doughnut shape that differs from a bell-shaped image in the absence of circulation (Amico, Osterloh, and Cataliotti, 2005); see Fig. 5. The value of the doughnut radius results in changing in discrete steps corresponding to the quantization of angular momentum of the condensate (Moulder *et al.*, 2012; Murray *et al.*, 2013; Wright *et al.*, 2013a; Ryu, Henderson, and Boshier, 2014); see Fig. 4(b).

An important readout of the current state of the system is provided by the heterodyne phase detection protocol (Corman *et al.*, 2014; Eckel, Jendrzejewski *et al.*, 2014; Mathew *et al.*, 2015). In this case, the ring condensate coexpands with a concentric disk condensate fixing a reference for the phase. The resulting image shows a characteristic spiral interferogram whose details (number of arms and sense of rotation) depend on the direction of current circulation. The spiral interferograms are also sensitive to the possible phase fluctuations along the ring (Corman *et al.*, 2014; Roscilde *et al.*, 2016). In this case, they display dislocations associated with phase slips; see Figs. 4(b) and 4(c). A minimally invasive technique based on the Doppler shift of the phonon modes of the condensate has been demonstrated to be effective in measuring the winding number (Kumar *et al.*, 2016).

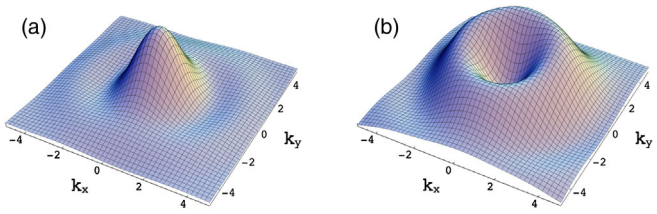

FIG. 5. TOF expansion of a ring-shaped condensate pierced by an effective magnetic field. The momentum distribution of a lattice system is displayed in the plane of the ring: $n(\mathbf{k}) = |w(\mathbf{k})|^2 \sum_{i,j} e^{-i(\mathbf{x}_i - \mathbf{x}_j)\cdot\mathbf{k}} \langle n \rangle$. The vectors $\mathbf{k} = (k_x, k_y)$ and $w(\mathbf{k})$ are Fourier transforms of the Wannier functions. (a),(b) Non-rotating and rotating condensates, respectively. Adapted from Amico, Osterloh, and Cataliotti, 2005.

For correlated systems on lattices, the phase information can be achieved by studying noise correlations in the expanding density (Haug, Tan *et al.*, 2018).

3. Persistent current in fermionic rings

The first analysis of a cold fermionic atom persistent current was carried out by Amico, Osterloh, and Cataliotti (2005). In their study, the fermions repel each other with a Hubbard interaction; see Eq. (6). Persistent currents of Fermi particles are subjected to parity effects. The currents behave diamagnetically or paramagnetically, depending on the parity of the number of particles on the ring (Leggett, 1991). The effect is due to the periodic boundary conditions imposed on the wave function. An explicit calculation with bosonization showed subtle effects of interactions and the effect of temperature (Loss, 1992). There is a critical temperature for the disappearance of the oscillations of the current as $k_B T = \hbar^2 m R^2$. In the case of interacting bosons, no parity effect occurs. In this case, the response is always paramagnetic (Pecci, Naldesi, Amico, and Minguzzi, 2021).

A readout of current states by interferometric means for fermions requires more attention (Pecci, Naldesi, Minguzzi, and Amico, 2021) than the bosonic case since all fermionic orbitals contribute to the interference pattern, giving rise to dislocations in the spiral interferograms. In addition, the time-of-flight images of circulating current states display a visible hole only if the circulating current is large enough to displace the entire Fermi sphere in momentum space (Pecci, Naldesi, Minguzzi, and Amico, 2021).

In the case in which attractive interactions occur among the particles, pairing or formation of higher-order bound states (quartets, many-body bound states) directly affects the persistent currents (Byers and Yang, 1961). The periodicity of the persistent currents scales as Φ_0/n, where n is the number of bound particles (Naldesi *et al.*, 2022). The curvature of the free energy at zero flux also displays a parity effect (Waintal *et al.*, 2008). In this case, it arises from a new branch in the ground-state energy (Pecci, Naldesi, Amico, and Minguzzi, 2021).

Like the attractive bosons, the periodicity of the persistent current of repulsive fermions in the strongly correlated regime is reduced by $1/N$. This effect is demonstrated through Bethe ansatz analysis for SU(2) (Yu and Fowler, 1992) and SU(κ) Fermi gases (Chetcuti, Haug *et al.*, 2022). This behavior is due to the phenomenon of spinon production in the ground state: spinons compensate for the increasing effective flux; since the spinons are quantized and the magnetic flux changes continuously, the compensation can be only partial. Therefore, an energy oscillation with characteristic periods smaller than the bare flux quantum Φ_0 is displayed. Even though the same $1/N$ reduction of the ground-state periodicity is found in strongly correlated attracting bosons (occurring as a result of formation of N-particle bound states in the "charge" quasimomenta), here we note that the "effective attraction from repulsion" resulting in SU(κ) systems arises because of the spin-spin correlations (Naldesi *et al.*, 2022). Finite temperature can affect the periodicity of a persistent current as the result of interplay between thermal fluctuations and interactions (Pâţu and Averin, 2022).

Finally, we note that, although the persistent current is mesoscopic in nature, it is demonstrated to display critical behavior when it undergoes the quantum phase transition from a superfluid to a Mott phase that, for $\kappa > 2$, occurs at a finite value of the interaction (Chetcuti, Haug *et al.*, 2022). Mott transitions in multiorbital SU(κ) Hubbard models were investigated by Richaud, Ferraretto, and Capone (2021, 2022). The first experimental demonstration of persistent current states in fermionic rings was recently reported (Cai *et al.*, 2022; Del Pace *et al.*, 2022). With a focus on attractive interactions, both homodyne and heterodyne interference in the BEC regime have been obtained. An in-depth theoretical analysis of interference fringes of SU(ν) fermions was carried out by Chetcuti, Osterloh *et al.* (2022).

C. Two-terminal quantum transport in cold-atom mesoscopic structures

In a typical two-terminal configuration, a mesoscopic region like a channel or a ring features quantum mechanical processes such as tunneling and interferences, and large leads characterized by their thermodynamic phases (which can be normal or superfluid) are connected to it with drive currents (Imry and Landauer, 1999); see Fig. 6(a).

1. Double-well systems

Two-terminal systems have been used with BECs to observe and manipulate phase coherence (Andrews *et al.*, 1997); see Dalfovo *et al.* (1999) for a detailed review. Conceptually, the simplest instance is a zero-temperature BEC in a double-well potential, as originally proposed by Smerzi *et al.* (1997). This system is of considerable interest from many perspectives, ranging from quantum metrology (Pezzè *et al.*, 2018) to quantum information processing (Haroche and Raimond, 2006). We restrict our discussion to atomic transport and refer the interested reader to the aforementioned reviews for in-depth discussions of the other aspects.

a. Tunnel regime

In this regime, we focus on the dynamics of the population imbalance in the two wells (Smerzi *et al.*, 1997), which is relevant for a high barrier (LeBlanc *et al.*, 2011; Spagnolli *et al.*, 2017). In the unbiased, noninteracting regime, the dynamics reduces to Rabi oscillations of the population across the barrier at the tunnel period (Spagnolli *et al.*, 2017). For increasing interactions and weak population imbalance, Rabi oscillations smoothly evolve into plasma oscillations, with a frequency controlled by the repulsion between atoms (Albiez *et al.*, 2005; Levy *et al.*, 2007; LeBlanc *et al.*, 2011; Pigneur *et al.*, 2018). For the largest imbalances, tunneling cannot compensate for the effect of the nonlinear interaction, leading to macroscopic quantum self-trapping (Albiez *et al.*, 2005; Levy *et al.*, 2007; Spagnolli *et al.*, 2017; Pigneur *et al.*, 2018). This dynamic occurs in the absence of dissipation, which is true in the two-mode regime at zero temperature (Gati *et al.*, 2006). For attractive interactions, the plasma oscillation mode softens down to zero frequency at a critical attraction (Trenkwalder *et al.*, 2016).

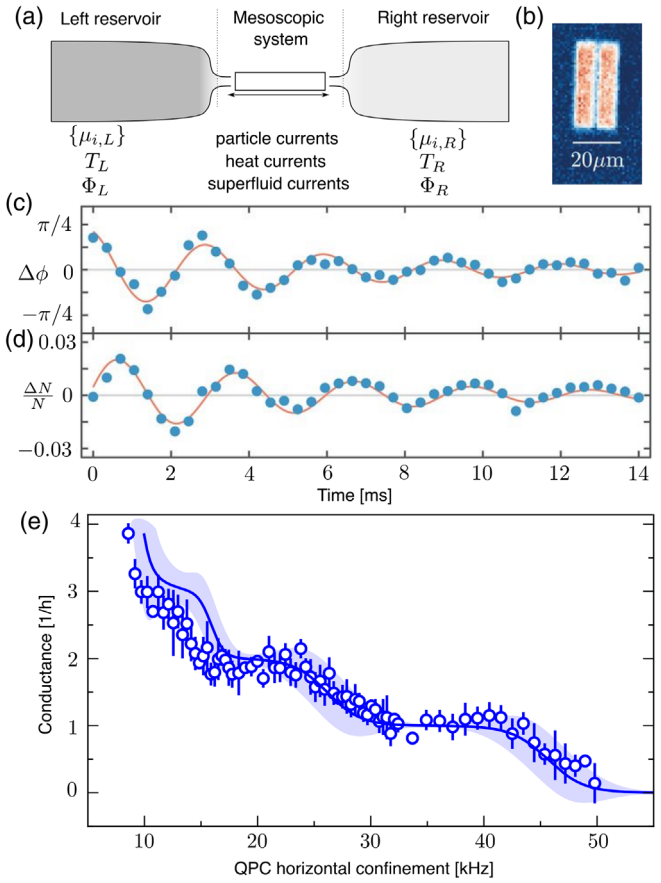

FIG. 6. (a) Two-terminal system comprising a mesoscopic system connected to reservoirs (L and R) with a set of control parameters: chemical potentials for species μ_i, temperature T, or superfluid phase Φ. (b) Two-terminal Josephson junction in a strongly interacting two-dimensional Fermi gas. (c) Phase difference and (d) atom number difference as a function of time in the junction after a relative phase difference of $\pi/4$ has been imprinted. (a)–(d) Adapted from Luick *et al.*, 2020. (e) Quantized conductance in a quantum point contact for weakly interacting fermions. Conductance is measured as a function of the quantum point contact (QPC) trap frequency (ν_x). The solid lines indicate predictions of the Landauer formula. Adapted from Krinner, Stadler, Husmann *et al.*, 2015.

The tunneling and interaction strength parameters of the two-mode model can be derived from the microscopic, mean-field Gross-Pitaevskii equation (Giovanazzi, Esteve, and Oberthaler, 2008; LeBlanc *et al.*, 2011) and depend on the details of the trap configuration. The predictions from this model are in good agreement with experiment (Ryu *et al.*, 2013). The fluctuations due to the discrete nature of atoms allows us to describe quantum fluctuations of the phase, similar to phase noise in a nonlinear interferometer (Pezzè *et al.*, 2018). Beyond the mean-field approximation in the strongly interacting regime, a rich phenomenology has been predicted (Zöllner, Meyer, and Schmelcher, 2008). Further quantum effects can also arise from continuous quantum measurements of the atom numbers (Uchino, Ueda, and Brantut, 2018).

b. Extended reservoirs

While the two-mode approximation captures the essence of superfluid atomic currents through a tunnel junction, it disregards processes that take place within the reservoirs. Large reservoirs feature excitations that can couple to the current. The double-well structure is a powerful configuration in which two identical systems can be produced and compared using interferometry. The internal dynamics of each system is then revealed in the phase relation between the two condensates. The latter has been used, in particular, for the study of one-dimensional gases in parallel wire configurations (Hofferberth *et al.*, 2007, 2008; Betz *et al.*, 2011; Gring *et al.*, 2012; Langen, Geiger, and Schmiedmayer, 2015). These landmark experiments reveal fine details of the effective field theory describing the one-dimensional reservoirs, including high-order correlations (Schweigler *et al.*, 2021). Allowing for a finite tunnel coupling between the two reservoirs modifies the effective sine-Gordon model describing the low-energy physics (Gritsev, Polkovnikov, and Demler, 2007). In a head-to-tail geometry (Polo *et al.*, 2018; Tononi *et al.*, 2020; Binanti, Furutani, and Salasnich, 2021), corresponding to the realization of the boundary sine-Gordon model, the Josephson oscillations are damped by the phonon bath in each wire, thereby realizing the Caldeira-Leggett model (Caldeira and Leggett, 1983).

The Josephson dynamics coupled with that of the reservoirs is captured phenomenologically by the resistively shunted Josephson junction model (Tinkham, 2012), inspired from the condensed-matter physics context and applied to atomtronic circuits by Eckel *et al.* (2016), Burchianti *et al.* (2018), and Luick *et al.* (2020). In this model, the reservoirs are described using an effective capacitance corresponding to the compressibility of the gas $C = \partial N/\partial\mu_r$, with μ_r the reservoir's chemical potential and N its atom number, derived from the equation of state and geometry.

Large reservoirs are also described using a kinetic inductance due to the finite mass of the atoms, which adds to that of the junction to form the total inductance L. The frequency $\omega_0 = (LC)^{-1/2}$ represents the first normal mode of the system, reducing to the dipole mode in a purely harmonic trap or to the plasma frequency in the two-mode model. The tunnel barrier itself is described by its critical current I_c, and the dissipative effects are captured by the parallel "shunt" resistance R. The superfluid character of the system is encoded in the current-phase relation of the tunnel barrier $I = I_c \sin\phi$ and the Josephson-Anderson equation relating the chemical potential difference $\Delta\mu$ to the phase $\dot{\phi} = \Delta\mu$ (Packard, 1998).

In this framework, the intrinsic properties of the superfluid junction can be studied independently of the dissipation by imposing a quasi-dc current (Levy *et al.*, 2007; Kwon *et al.*, 2020). Alternatively, imprinting a phase difference across the junction by applying an external bias for a short time and measuring the current response through the junction realizes the equivalent of the dc Josephson effect (Luick *et al.*, 2020).

At nonzero temperature, thermally excited atoms serve as a natural source of dissipation justifying a finite value for R (Ruostekoski and Walls, 1998; Zapata, Sols, and Leggett, 1998; Marino *et al.*, 1999; Levy *et al.*, 2007). Even at zero temperature, a finite damping arises as the current couples to the internal dynamics of the reservoirs. In weakly interacting BECs and in Fermi gases in the BEC-BCS crossover, the

physics captured by the resistance is related to the nucleation of topological defects (Wright *et al.*, 2013a; Jendrzejewski *et al.*, 2014; Valtolina *et al.*, 2015; Eckel *et al.*, 2016; Li *et al.*, 2016; Burchianti *et al.*, 2018; Xhani *et al.*, 2020) or phase slips in one dimension (Polo *et al.*, 2019; Dubessy *et al.*, 2021). The current also couples to Bogoliubov excitations in BECs and superfluid Fermi gases (Luick *et al.*, 2020; Singh *et al.*, 2020), competing with the coupling to vortices at higher temperature (Singh *et al.*, 2020). The coupling of tunneling with the Bogoliubov spectrum was theoretically studied by Meier and Zwerger (2001), Uchino (2020), and Uchino and Brantut (2020), predicting a finite dc resistance at zero temperature.

Fermi superfluids also feature pair-breaking excitations, which have spectacular effects on the transport properties (Averin and Bardas, 1995). Indirect evidence for such effects has been reported with cold Fermi gases in a point contact (Husmann *et al.*, 2015). The Ambegaokar-Baratoff formula relating pair-breaking excitations to the critical current in weakly interacting fermionic superfluids is shown to smoothly interpolate with dissipation induced by Bogoliubov excitations in the crossover from BCS to BEC (Zaccanti and Zwerger, 2019). Deeply within the scopes of atomtronics, the Josephson dynamics can be used to probe bulk quantum properties of the materials such as the superfluid order parameter (Kwon *et al.*, 2020) or flat-band superconductivity (Pyykkönen *et al.*, 2021).

c. Weak links in interacting systems

In this regime, both the junction and the reservoirs have a macroscopic size compared to the coherence or healing length of the gas. In such a weak link an appropriate description of transport can be obtained using superfluid hydrodynamics. It incorporates the transport of noninteracting thermal excitations (Papoular, Pitaevskii, and Stringari, 2014). A lump element model can be derived from the microscopic hydrodynamics in a rigorous way for weakly interacting bosons, leading to accurate predictions for the dynamics of two-terminal systems (Gauthier *et al.*, 2019). In general, the population oscillations between reservoirs (Papoular, Pitaevskii, and Stringari, 2014) and that of the superfluid phase closely matches the plasma oscillation in the two-mode approximation. There dissipation arises due to phase slippage mechanisms occurring within the weak link, and no qualitative difference emerges for long channels compared to tunnel-like barriers (Beattie *et al.*, 2013; Wright *et al.*, 2013a; Jendrzejewski *et al.*, 2014; Eckel *et al.*, 2016; Burchianti *et al.*, 2018; Xhani *et al.*, 2020).

The case of superfluid Fermi gases has been studied in this context through a direct comparison between the unitary gas and a noninteracting Fermi gas, showing differences of two orders of magnitude in the conductance (Stadler *et al.*, 2012). Furthermore, long channels can feature sections exposed to a tailored potential such as disorder. In a strongly interacting superfluid, a crossover is observed between a low disorder regime with superfluid transport and a disorder-dominated regime with low conductance (Krinner *et al.*, 2013; Krinner, Stadler, Meineke *et al.*, 2015).

2. Conductance measurements and incoherent reservoirs

In situations where quantum coherence either is nonexistent or can be neglected such as in junctions dominated by dissipation, transport is captured by the conductance $G = I/\Delta\mu$, where $\Delta\mu$ is the chemical potential difference between the two reservoirs.

a. Noninteracting atoms

For reservoirs of noninteracting particles or quasiparticles, the current is determined by the energy-dependent transmission coefficients of the junction $\mathcal{T}_n$, where n labels the transverse modes of the junctions, through the Landauer formalism (Cuevas and Scheer, 2017)

$$I = \frac{1}{h}\int d\epsilon \sum_n \mathcal{T}_n(\epsilon)[f_1(\epsilon) - f_2(\epsilon)], \tag{8}$$

where f_1 and f_2 are the energy distributions of particles in the two reservoirs. For Fermi gases and liquids, f is the Fermi-Dirac distribution corresponding to the reservoir chemical potential μ_i and temperatures T_i. The formalism also applies to weakly interacting bosons above the critical temperature (Nietner, Schaller, and Brandes, 2014; Papoular, Pitaevskii, and Stringari, 2016; Kolovsky, Denis, and Wimberger, 2018). The strength of the Landauer paradigm is the separation between the quantum-coherent part and the incoherent reservoirs, with the latter featuring fast dissipation processes that are not described microscopically. The atomtronic Laudauer setup, with control over the reservoir properties, has provided motivation for detailed theoretical studies of the dissipation dynamics through a comparison of the various microscopic descriptions (Ivanov *et al.*, 2013; Chien, Di Ventra, and Zwolak, 2014; Gallego-Marcos *et al.*, 2014; Nietner, Schaller, and Brandes, 2014; Kolovsky, 2017).

The Landauer paradigm was proposed for cold atoms by Bruderer and Belzig (2012) and Gutman, Gefen, and Mirlin (2012) and independently realized experimentally by Brantut *et al.* (2012) using weakly interacting fermions in two reservoirs connected by a mesoscopic, quasi-two-dimensional constriction. For tight constrictions, the system behaves as a simple *RC* circuit, with capacitors modeling the reservoirs and the constriction the resistance. Measuring the decay constants of an initially prepared particle-number imbalance between the two reservoirs and inferring the compressibility from the equation of state allowed researchers to extract the conductance of the constriction. Early experiments focused on variations of conductance induced by changes of shape of the constriction or the introduction of disorder (Brantut *et al.*, 2012). In recent experiments a similar system was used to investigate Anderson localization effects in two dimensions (White *et al.*, 2020).

At zero temperature and low chemical potential difference, Eq. (8) yields $I = \Delta\mu/hj$, where j is an integer. Each mode energetically accessible in the conductor contributes independently by $1/h$ to the conductance. In experiments, this is manifested in jumps of the conductance by $1/h$ as the Fermi energy reaches the successive transverse modes of the constriction, as observed in condensed-matter devices (van Wees *et al.*, 1988; Wharam *et al.*, 1988) and in an atomtronic

context (Krinner, Stadler, Husmann *et al.*, 2015), as shown in Fig. 6.

On top of such an ideal one-dimensional conductor, high-resolution optical methods allowed for the projection of structures described in Sec. II.C.3, such as pointlike scatterers. Measuring the conductance as a function of the scatterer's location produces a high-resolution spatial map of the transport process, akin to scanning gate microscopy in the condensed-matter context (Häusler *et al.*, 2017). Disposing several scatterers in a regular fashion produced a mesoscopic lattice that exhibits a band structure directly observed in the transport properties, demonstrating the ability to observe and control quantum interference at the single scatterer level (Lebrat *et al.*, 2018).

The notions of reservoirs and channels can be interpreted in a more abstract way through the concept of synthetic dimension using internal states of atoms (Celi *et al.*, 2014) or vibrational states of traps (Price, Ozawa, and Goldman, 2017). The two-terminal transport concept has also found a generalization through this mapping: a spin imbalanced Fermi gas provides a realization of two terminals in the spin space, and an impurity with engineered spin-changing collisions provides the counterpart of a point contact (You *et al.*, 2019). The use of vibrational states of reservoirs and constrictions as a synthetic dimension then allows us to envision synthetic multiterminal situations, where transport would be sensitive to chirality (Salerno *et al.*, 2019).

b. Incoherent transport of interacting atoms

The situation involving quantum point contacts and one-dimensional constrictions in the presence of interactions has been thoroughly investigated in the condensed-matter physics context (Imry, 2002; Cuevas and Scheer, 2017). For two-terminal atomtronic systems, this situation was theoretically envisioned for bosons by Gutman, Gefen, and Mirlin (2012) with ideal reservoirs and by Simpson *et al.* (2014) with superfluid reservoirs in the framework of Luttinger liquid physics. For fermions, the point contacts and wires have been experimentally investigated in the deep superfluid regime for a unitary Fermi gas (Husmann *et al.*, 2015), showing nonlinear current-bias relations that could be traced back to multiple Andreev reflections (Krinner, Esslinger, and Brantut, 2017). This regime is expected to interpolate continuously with the Josephson regime as the transmission in the point contact is reduced (Averin and Bardas, 1995; Yao *et al.*, 2018). This was further investigated by continuously increasing interactions from the free Fermi gas, showing quantized conductance, up to unitarity with a nonlinear response (Krinner *et al.*, 2016). In the intermediate regime, the conductance plateau is observed to increase continuously from $1/h$ up to values as high as $4/h$ before disappearing close to unitarity, which could be due to either confinement induced pairing within the contact (Kanász-Nagy *et al.*, 2016; Liu, Zhai, and Zhang, 2017) or superfluid fluctuations in the reservoirs (Uchino and Ueda, 2017).

Transport in the one-dimensional lattice, featuring a band structure, offers the possibility of exploring the fate of metallic and insulating behavior as interactions are varied (Lebrat *et al.*, 2018). It was found that the band insulator evolves smoothly into a correlated insulator comprising bound pairs with unit filling in the lattice, as interactions are increased, thus providing evidence for the Luther-Emery phase (Giamarchi, 2003).

c. Spin and heat transport

Transport in the two-terminal system can be generalized to spin in a two-component Fermi gas, where the total magnetization is conserved and can be exchanged between two reservoirs. The linear response in currents is expressed through a matrix relating the currents of the two spin components to their respective chemical potential biases, with off-diagonal elements describing spin drag. In contrast to particle conductance, magnetization currents are sensitive to interactions since collisions do not conserve the total spin current. Even in the absence of a constriction or channel, two clouds of opposite polarization relax slowly to equilibrium, especially at unitarity (Sommer *et al.*, 2011), where the spin diffusion coefficient saturates to a universal value. These experiments have been repeated for a metastable, strongly repulsive Fermi gas, providing evidence for a ferromagnetic instability (Valtolina *et al.*, 2017). In the case of a one-dimensional quantum wire, the strongly attractive Fermi gas is found to behave as an ideal spin insulator, as a consequence of pairing (Krinner *et al.*, 2016). Another possibility to manipulate spin currents is created by the use of spin-dependent potentials, which are used to produce a spin valve from a quantum point contact (Lebrat *et al.*, 2019).

Heat and energy transport can be investigated by introducing a temperature bias between the two reservoirs and observing energy flow through the channel. Heat and particle currents couple both through the thermodynamics of the reservoir due to finite dilation coefficients and through the genuine thermoelectric effect originating from the energy dependence of the transmission coefficient, as observed by Brantut *et al.* (2013) and Häusler *et al.* (2021). This also opens the perspective of Peltier cooling methods for quantum gases (Grenier, Georges, and Kollath, 2014; Grenier, Kollath, and Georges, 2016; Sekera, Bruder, and Belzig, 2016). In the case of the unitary Fermi gas, a similar experiment on quasi-one-dimensional constrictions was performed, yielding a low heat conductance and a breakdown of the Wiedemann-Franz law, in qualitative agreement with theory (Pershoguba and Glazman, 2019), but a thermopower compatible with that of a noninteracting Fermi gas (Husmann *et al.*, 2018). Such a breakdown was also predicted for strongly interacting bosons within the Luttinger liquid framework (Filippone, Hekking, and Minguzzi, 2016).

d. Dissipative barriers

As opposed to electrons, atomtronic devices allow for the engineering of atom losses. This has been investigated using electron microscopy with the creation of highly localized purely dissipative barriers (Barontini *et al.*, 2013; Labouvie *et al.*, 2015). The non-Hermitian character of the resulting Hamiltonian supports the observation of coherent perfect absorption (Müllers *et al.*, 2018). Using an optical barrier involving spontaneous emission also produces dissipation in addition to the optical potential. This was studied by

Corman *et al.* (2019). The interplay of these effects with interactions and fermionic superfluidity was investigated by Damanet *et al.* (2019a).

3. Two-terminal transport through ring condensates

Transport in circuits with closed architectures provides a direct way to explore the coherence of the system (Imry, 2002). At the same time, it provides an instance of integrated atomtronic circuits. Consider particles injected from a source into a ring-shaped circuit pierced by an effective magnetic field and collected in a drain lead. The phase of particles couples there with the gauge field and the transport displays characteristic Aharonov-Bohm interference patterns (Aharonov and Bohm, 1959; Leggett, 1980; Olariu and Popescu, 1985; Vaidman, 2012), as studied in electronic systems (Büttiker, Imry, and Azbel, 1984; Gefen, Imry, and Azbel, 1984; Webb *et al.*, 1985; Jagla and Balseiro, 1993; Marquardt and Bruder, 2002; Nitzan and Ratner, 2003; Hod, Baer, and Rabani, 2006; Lobos and Aligia, 2008; Rincón, Hallberg, and Aligia, 2008; Rincón, Aligia, and Hallberg, 2009; Shmakov, Dmitriev, and Kachorovskii, 2013).

Atomtronics allows the study of transport through ring-shaped circuits in new ways, with carriers of various statistics, tunable atom-atom interactions, and lead-ring couplings (Haug, Dumke *et al.*, 2019a; Haug, Heimonen *et al.*, 2019). Specifically, the nonequilibrium dynamics described by the Bose-Hubbard or discrete Gross-Pitaevskii model is analyzed by quenching the particles' spatial confinement in both closed and open configurations. Depending on the ring-lead coupling, interactions, and particle statistics, the system displays qualitatively distinct nonequilibrium regimes with different responses of the interference pattern to the effective gauge field. In contrast to fermionic systems, the coherent transport of strongly interacting bosons does not display characteristic oscillations as a function of the effective magnetic flux. A possible explanation for the suppression of the Aharonov-Bohm oscillations comes as a compensation between the phase of the condensate and the Aharonov-Bohm phase. For a field theoretic explanation for the absence of Aharonov-Bohm interference in the circuit, see Tokuno, Oshikawa, and Demler (2008).

The transport through the lead-ring interface can display a bosonic analog of Andreev scattering: when a bosonic matter wave hits the lead-ring interface, it is transmitted to the ring with the emission of a matter wave of negative amplitude, a "hole," that is reflected backward (Daley, Zoller, and Trauzettel, 2008; Watabe and Kato, 2008; Zapata and Sols, 2009). Two-terminal transports through rings and Y junctions were considered by Haug, Dumke *et al.* (2019a).

Coherent transport can also be achieved through topological pumping by driving a system protected by a band gap periodically in time (Thouless *et al.*, 1982; Thouless, 1983). Such periodic drives are natural in atomtronics thanks to the availability of reconfigurable circuits (McGloin *et al.*, 2003; Gaunt and Hadzibabic, 2012; Gauthier *et al.*, 2016). Topological pumping through source-ring-drain atomtronic circuits was addressed by Haug, Dumke *et al.* (2019b). This way, topological bands and the Aharonov-Bohm effect in interacting bosonic systems are intertwined: the Aharonov-Bohm interference affects reflections by inducing specific transitions between topological bands. The system effectively works as a nonlinear interferometer in which the source ring and the ring drain act as beam splitters. The interaction adjusts the transmission and reflection coefficients and entangles the propagating wave functions in the two arms of the interferometer.

IV. ATOMTRONIC COMPONENTS AND APPLICATIONS

In this section, we discuss the atomtronic circuital elements that have been considered in the literature. Sections IV.A and IV.B concern the atomic analogs of certain circuit elements in classical electronics. Sections IV.C and IV.D address atomtronic qubits inspired by quantum electronics. Section IV.E focuses on atomtronic interferometers.

A. Matter-wave optics in atomtronic circuits

Transport in atomtronic circuits can be either coherent transmission–like in photonic circuits or more like a superfluid (similar to superconducting electronics). A classical example is the decay of superfluid currents described in Sec. III.B. The main stumbling block in observing the coherent transmission of matter waves over macroscopic distances is the degree of roughness of the waveguides that are currently available.

Until recently, except for straight guides formed by collimated laser beams, atomtronics has been limited to the latter. This situation changed recently with the first demonstration of coherent guiding over macroscopic distances in a ring-shaped matter-wave guide (Pandey *et al.*, 2019). It is now possible to (de)accelerate BECs in an optimal way toward speeds of many times the critical superfluid velocity and an angular momentum exceeding $40\,000\hbar$ per atom without observable decay over time. Matter-wave lensing and delta-kick cooling (Arnold, MacCormick, and Boshier, 2002; Kovachy *et al.*, 2015) have now been demonstrated using gravitomagnetic lenses inside of TAAP matter-wave guides, where BECs and thermal clouds have been collimated, thus reducing their expansion energies by a factor of 46 down to 800 pK (Pandey *et al.*, 2021). Delta-kick cooling with an optical potential is routinely used in waveguide atom interferometers to lower the energy of an expanded and collimated BEC below a few nanokelvins (Krzyzanowska *et al.*, 2022).

B. Transistors, diodes, and batteries

Early work in atomtronic devices sought to emulate semiconductor material-based elements by considering neutral atoms in optical lattices (Seaman *et al.*, 2007; Pepino *et al.*, 2009; Pepino, 2021), but work also sought simply functional duals by considering atoms confined to a small number of potential wells (Stickney, Anderson, and Zozulya, 2007). There are substantial differences in the underlying physics, as well as practical differences, between these two approaches to device design.

Lattice-based devices share clear analogies with electronic systems in periodic potentials characterized by band structure effects. At the same time, bosonic many-particle systems are unavoidably characterized by specific quantum correlations,

making their dynamics distinct from the electronic one. Specifically, lattice-based atomtronic components deal with superfluids (instead of conductors) and heavily rely on the possibility of engineering a Mott insulating quantum phase that interacting bosons can undergo for integer filling fractions (the number of bosons commensurate with the number of lattice points). Another effect without any classical electronics analog is the macroscopic quantum self-trapping phenomenon that can hinder the transmission of a bosonic fluid through a potential barrier (Milburn *et al.*, 1997; Smerzi *et al.*, 1997). As a specific example of the semiconductor approach, an atomtronic diode can be conceived in analogy with the electronic *P*-*N* junction diode: the different concentration of electrons and holes in the *P* and *N* materials set a potential drop that can be modulated by an external voltage bias. The so-called forward (reverse) bias corresponds to a reduction of the potential drop for the electrons (holes) at the junction, and therefore particle flow takes place. In the atomtronic diode, the junction is realized by facing commensurate and incommensurate lattices of condensates: an abrupt change of the chemical potential at the junction, which plays the role of the voltage bias (Pepino *et al.*, 2009). This way, the control of the chemical potential can make the bosons move from the commensurate to the incommensurate lattice of the condensate, but not vice versa. The diode may be connected to two bosonic reservoirs kept at different chemical potentials that play the role of the battery. Ultimately, the nonlinear device behavior arises from the nonlinearity of the atom-atom interactions, which is a feature specific to the lattice systems.

Here we note that classical electronic circuits are indeed non-thermal-equilibrium systems whose dynamics is entirely driven by the presence of a battery (or another source of electric potential) supplying power to the circuit. It is also significant that a battery is fundamentally associated with an internal resistance, which causes the battery to dissipate energy. In atomtronic circuits, it is a BEC with finite chemical potential and temperature that serves to provide the "bias" driving the nonequilibrium dynamics of a circuit. And like the electrical battery, a BEC-based battery providing atom current to a circuit will exhibit an internal resistance. While the classical battery is always associated with a positive resistance, an atomtronic (BEC) battery can exhibit either positive or negative internal resistance, depending on whether the supplied current is thermal or condensed, respectively (Zozulya and Anderson, 2013). An experimental study of atomtronic batteries was carried out by Caliga, Straatsma, and Anderson (2017).

A battery not only powers a circuit but is necessary to provide the gain associated with transistor action. This action has been studied in a semiclassical context utilizing a triple-well atomtronic transistor in an oscillator configuration; see Fig. 7 (Stickney, Anderson, and Zozulya, 2007; Caliga *et al.*, 2016). The leftmost well acts as the source, the middle as the gate, and the right as the drain, where the nomenclature is taken from the electronic field-effect transistor. Here the system is initialized by placing a BEC at a given temperature and chemical potential in the source well.

The transistor circuit behavior is characterized by a critical feedback parameter given by a normalized difference in barrier height (Caliga *et al.*, 2012): $\upsilon = (V_{\mathrm{GD}} - V_{\mathrm{GS}})/k_B T_S$,

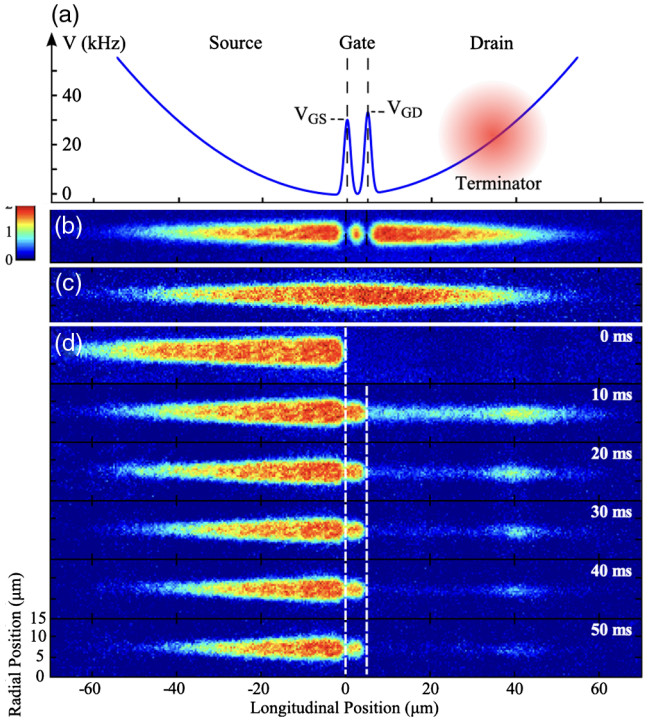

FIG. 7. Atomtronic triple-well transistor. (a) Atomic potential consisting of a hybrid magnetic confinement combined with barriers superimposed by the optical projection of a pair of blue-detuned laser beams. A "terminator" laser beam removes atoms from the drain by pumping them to an untrapped m_F state. The gate width is 4.5 μm. Thermal atoms are loaded in (b) the hybrid potential and (c) in the absence of optical barriers. (d) Absorption images of the atoms in the wells at various evolution times, starting at $t = 0$ ms and ending at 50 ms. Adapted from Caliga, Straatsma, and Anderson, 2016.

in which T_S is the temperature of the source atoms, and V_{GD} and V_{GS} are the barrier heights; see Fig. 7. A semiclassical kinetic treatment has been developed in which the atoms are treated as particles while they are also allowed to Bose condense under appropriate conditions. With such an approach, the BEC spontaneously developed in an initially empty gate well when the feedback exceeded a threshold value (Caliga *et al.*, 2012). This is reflected in the data of Fig. 7 where a high density of atoms appears in the gate at 10 ms evolution time [in fact the high density is apparent after only 1 ms (Caliga, Straatsma, and Anderson, 2016)]. The transport semiclassical dynamics of the transistor coupled to the environment, in which the atom steady currents are driven by the chemical potentials, was studied by Caliga *et al.* (2016). In particular, by analyzing the gain as a function of the operating condition, it was proved that such an atomtronic component can be be used to supply power to a given load (therefore acting as an active component).

C. The atomtronic quantum interference device

A toroidal circuit of ultracold atoms interrupted by tunnel junctions provides the atomic counterpart of the SQUID: the atomtronic quantum interference device (AQUID). AQUIDs with the characteristic control of noise and interactions and a

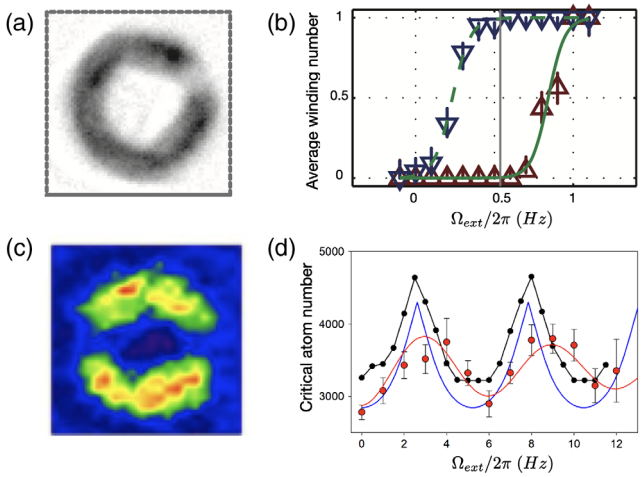

FIG. 8. Fabricated AQUIDs. (a) rf AQUID of the NIST group. (b) Hysteretic property of the rf AQUID. (c) dc AQUID realized by the Los Alamos group. (d) Oscillations of the critical current demonstrating a superposition of superfluid currents. The black and blue curves are theoretical expectations and the error bars are results from the experiment, with the red curve a best fit of it. (a), (b) Adapted from Eckel, Lee *et al.*, 2014. (c) Adapted from Ryu *et al.*, 2013. (d) Adapted from Ryu, Samson, and Boshier, 2020.

low decoherence of neutral ultracold matter enclose a great potential for both basic science and technology. AQUID realized by a toroidal-shaped superfluid Bose-Einstein condensate obstructed using a rotating weak link was carried out by the National Institute of Standards and Technology (NIST) (Eckel, Lee *et al.*, 2014); see Fig. 8(a). By analogy with the radio-frequency SQUID, this rf AQUID displays hysteresis in angular momentum; see Fig. 8(b). The role of the vortices generated by the stirring barrier (Yakimenko *et al.*, 2014, 2015) or thermal fluctuations (Kumar *et al.*, 2017; Kunimi and Danshita, 2019; Mehdi *et al.*, 2021) have been analyzed. Barrier strength and the dynamical protocol of ramping up and down the stirring potential need to be carefully chosen to achieve a controlled and effective realization of the AQUID (Mathey and Mathey, 2016). The readout of the rf AQUID in the different regimes of interaction and barrier strength was studied by Haug, Tan *et al.* (2018), who monitored the dynamics of interference fringes established after the condensate is released.

Toroidal-shaped condensates interrupted by two tunnel junctions have been experimentally fabricated by the Los Alamos group through the painting technique described in Sec. II.A.2 (Ryu *et al.*, 2013); see Fig. 8(c). This system, which provides the atomtronic counterpart of the direct-current SQUID, is referred to as dc AQUID. Following Giovanazzi, Smerzi, and Fantoni (2000) the dc Josephson effect in the experiment arises when the atom density (chemical potential) remains constant in each sector of the torus despite the two barriers moving circumferentially toward each other. Indeed, the current increases with barrier velocity until the critical current of the junctions is reached. At this point the system switches to the ac Josephson regime characterized by an oscillating Josephson current. The frequency of the oscillations turns out to be proportional to the chemical potential difference across the junction, but there is no net current across it. The critical current is observed to display characteristic oscillations demonstrating the superposition of superfluid currents; see Fig. 8(d).

The interference of persistent currents of dc AQUIDs was recently carried out experimentally (Ryu, Samson, and Boshier, 2020). By inducing a bias current in a rotating atomic ring interrupted by two weak links, one finds that the interference between the Josephson current with the current from the rotation creates a oscillation in the critical current with applied flux. This oscillation is measured experimentally in the transition from the dc to the ac Josephson effect. This experiment was performed within a dilute Bose-Einstein condensate that is well described within a mean-field description, and thus entanglement of currents, which is a key ingredient for the atomic qubit, has not been demonstrated. Nonetheless, it is a major step toward the implementation of the atomic qubit.

D. Atomtronic qubit implementations

Atomtronic qubit implementations have been proposed to combine the logic of cold-atom-based and superconducting circuit–based qubits. The basic idea is to use the persistent currents of cold-atom systems flowing in ring-shaped potentials. To have two well-defined energy levels, the translational invariance of the system needs to be broken by the insertion of suitable weak links. The presence of the weak link breaks the axial rotational symmetry of the ring fluid and couples different angular momenta states, opening a gap at the degeneracy point among two angular momentum states; see Sec. III.B.1. This way the two states of the qubit system are the symmetric and antisymmetric combinations of the two angular momentum states (Amico, Osterloh, and Cataliotti, 2005; Solenov and Mozyrsky, 2010; Amico *et al.*, 2014; Aghamalyan *et al.*, 2015, 2016). The nature of the superposition state depends on the system parameters: at weak interactions it is a single-particle superposition, at intermediate interaction a quantum mechanical many-body entangled–like state, and at strong interactions a "Moses state," i.e., a superposition of Fermi seas (Hallwood, Burnett, and Dunningham, 2006; Nunnenkamp, Rey, and Burnett, 2008; Schenke, Minguzzi, and Hekking, 2011). An important point in this context is to establish to what extent the cold-atom quantum technology would be capable of feasibly addressing the qubit. In particular, the energy gap separating the two energy levels of the qubit displays a specific dependence on the number of atoms in the ring network, the atom-atom interaction, and the atom tunneling rates through the weak link (Nunnenkamp, Rey, and Burnett, 2011). The numerical analysis based on the BHM shows that the limit of a weak barrier and intermediate to strong interactions forms the most favorable regime: a qubit regime; see Fig. 9 (Amico *et al.*, 2014; Aghamalyan *et al.*, 2016). The spectral quality of the qubit was analyzed by Aghamalyan *et al.* (2015) as a function of the physical parameters of the system. The three-weak-link architecture (Aghamalyan *et al.*, 2016) indeed realizes a two-level effective dynamics in a considerably enlarged parameter space. Machine learning preparation of an entangled persistent current was demonstrated by Haug *et al.* (2021).

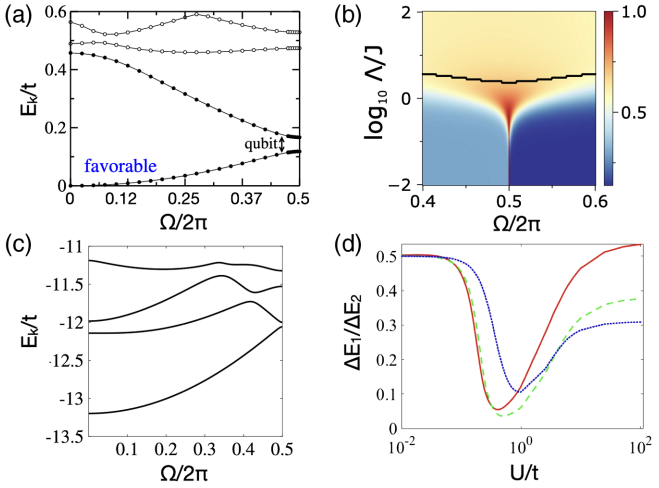

FIG. 9. Atomtronic qubits. Top panels: Bose-Hubbard rings interrupted by a single weak link. Bottom panels: flux qubit configuration of a Bose-Hubbard ring interrupted by three weak links. (a),(c) Energy levels E_k. (b) Noise correlations in the TOF image of the single-weak-link qubit. Adapted from Haug, Tan *et al.*, 2018. (d) Summary of the qubit quality factor as provided by the ratio between the energy gaps between the ground-state energy and the first two excitation energies ΔE_1 and ΔE_2. (a) Adapted from Aghamalyan *et al.*, 2015. (c),(d) Adapted from Aghamalyan *et al.*, 2016.

The analysis based on the QPM working in the limit of a large number of particles is important for the aforementioned feasibility of the qubit dynamics; see Eq. (3). Here the two-level qubit dynamics emerges analytically (Amico *et al.*, 2014). In the case of a ring circuit interruped by a single weak link, the effective Hamiltonian is $\mathcal{H}_{\rm eff} = \mathcal{H}_{\rm syst} + \mathcal{H}_{\rm bath} + \mathcal{H}_{\rm syst\text{-}bath}$, in which $\mathcal{H}_{\rm syst} = U\boldsymbol{n}^2 + E_L\boldsymbol{\varphi}^2 - E_J\cos(\boldsymbol{\theta} - \Omega)$, where θ is the phase slip across the weak link, with $E_L = J/M$, and $E_J = J'$. For $\delta \doteq E_J/E_L \geq 1$, $\mathcal{H}_{\rm syst}$ describes a particle in a double-well potential. $\mathcal{H}_{\rm bath}$ describes the dissipative dynamics $\mathcal{H}_{\rm syst\text{-}bath}$ and the interaction due to the phase slips occurring in the other lattice sites; see also Rastelli, Pop, and Hekking (2013).

The qubit can be probed through a Rabi-type protocol. By quenching the effective magnetic field to the degeneracy point, characteristic Rabi oscillations occur with a frequency $\propto 1/\Delta E_1$ (Schenke, Minguzzi, and Hekking, 2011; Polo *et al.*, 2022). The two states of the qubit could be manipulated through a suitable "pulse" of the artificial magnetic field.

The readout has been studied with various expanding condensate protocols (Aghamalyan, 2015; Haug, Tan *et al.*, 2018). In particular, the two-level system structure and the corresponding specific entanglement between the clockwise and counterclockwise flows can be quantified through the noise in the momentum distribution $\langle\hat{n}(\mathbf{k})\hat{n}(\mathbf{k})\rangle - \langle\hat{n}(\mathbf{k})\rangle\langle\hat{n}(\mathbf{k})\rangle$, resulting in the maximum at the degeneracy point; see Fig. 9(b) (Haug, Tan *et al.*, 2018).

Proofs of concept for qubit coupling have been provided in which qubits are imagined to be arranged in stacks (Amico *et al.*, 2014) or in a planar configuration (Safaei *et al.*, 2018). Reliance on recent optical circuit designs allows much more flexible solutions to be implemented (Rubinsztein-Dunlop *et al.*, 2017).

E. Atomtronic interferometers

An interferometer splits a wave function into a superposition of two parts and then recombines them in a phase-coherent fashion. If the wave packets overlap perfectly at the output of the interferometer, the phase difference between the two arms is the difference between the phase shifts imposed by the pulsed beam splitters and the mirrors in each arm plus the propagation phase $\Delta\phi_{\rm prop} = (S^1 - S^2)/\hbar$, where S^i is the classical action computed along the path i (Peters, Chung, and Chu, 2001). A beam splitter at the interferometer transforms the phase difference into a population difference, which is easily read out. Most of the atom interferometer solutions demonstrated to date have involved free-falling atoms Traditional atom interferometers involve free-falling atoms (Müller *et al.*, 2008; Arimondo *et al.*, 2009; van Zoest *et al.*, 2010; Geiger *et al.*, 2011, 2020; Stockton, Takase, and Kasevich, 2011; Sugarbaker, 2014; Bongs *et al.*, 2019). They have the advantage of decoupling the atoms from many effects that might otherwise cause uncontrollable additional phase shifts, which could lead to a deterioration of contrast or a random shift of the fringes. The main disadvantage is the size of the interferometer: Longer interrogation times lead to larger phase shifts. Therefore, free-falling high-precision matter-wave interferometers need to be tall in order to accommodate the distance that the atoms fall during the interrogation, reaching a size of 10 or even 100 m (Muntinga *et al.*, 2013; Kovachy *et al.*, 2015). In contrast, atomtronic interferometers use a trapping or guiding potential (usually magnetic or dipole) to compensate for gravity and thus can achieve a much increased detection time with much reduced space requirements. This comes, however, at the cost of an increased risk of noise and systematic effects due to fluctuations in the guiding potential.

1. Sagnac effect–based atomtronic sensors

An important application of waveguide atom interferometer gyro-technology is inertial navigation in the absence of position information provided by a global navigation satellite system. An inertial navigation system (INS) contains three accelerometers whose output is integrated twice to get displacement, along with three gyros that track the orientation of the accelerometers. It turns out that the navigation accuracy of current INS over timescales of hours and longer is limited by the drift in the zero of the gyros. These sensors are usually fiber-optic gyros (FOGs). Free-space atom interferometer gyros have already demonstrated extremely low drift (Gustavson, Bouyer, and Kasevich, 1997; Gustavson, Landragin, and Kasevich, 2000; Helm, Cornish, and Gardiner, 2015), with their main disadvantage for some applications being the large physical size required to accommodate a free fall of atoms that are interrogated over several seconds. Guided atom interferometer gyros analogous to the FOG would be much more compact, making them attractive for navigation if they can be engineered to have low drift.

In a typical rotation-sending configuration, atomtronic high-precision gyros are based on the Sagnac effect. Two input quantum waves propagating along two different arms of a closed path circuit of enclosed area A produce interference fringes at the interferometer output; if the circuit is rotated at rate Ω, the interference fringes will be shifted by

$$\Phi_{\mathrm{Sagnac}} = \frac{4\pi E}{hc^2}\mathbf{A}\cdot\mathbf{\Omega}, \tag{9}$$

where E is the energy of the traveling wave and $\mathbf{A}$ and $\mathbf{\Omega}$ are the enclosed area and the rotation vector, respectively. For frequency ν photon-based Sagnac interferometers, $E_{\mathrm{ph}} = h\nu$, and for matter waves it is $E_{\mathrm{mw}} = mc^2$ instead, yielding $\Phi_{\mathrm{Sagnac}} = [4\pi/(h/m)]\mathbf{A}\cdot\mathbf{\Omega}$. For equal particle flux and enclosed area, the difference in sensitivity between photon and matter-wave interferometers is thus the ratio between the energies $E_{\mathrm{mw}}/E_{\mathrm{ph}} = 10^{10}$. Light-based interferometers typically contain orders of magnitude more photons than the matter-wave interferometers contain atoms. They also tend to enclose a much larger area. Nevertheless, matter-wave interferometers are expected to outperform their photon counterparts, such as where long-term stability is required.

2. Bright soliton rotation sensors

A BEC with attractive interactions (such as ^{85}Rb or ^{7}Li) in a ring-shaped guide can realize bright soliton interferometry. A localized barrier can split the solitons into two waves propagating in clockwise and counterclockwise directions that can ultimately recombine after traveling two semicircles. Even though perfect bright solitons can go through each other without changing their density profiles, the two waves can provide a Sagnac phase shift (Helm, Billam, and Gardiner, 2012; Polo and Ahufinger, 2013; McDonald *et al.*, 2014; Helm, Cornish, and Gardiner, 2015). The splitting of bright solitons scattering on a localized barrier was analyzed by Weiss and Castin (2009), Helm *et al.* (2014), and Marchukov *et al.* (2019). In such a process, superposition states are predicted to occur (Streltsov, Alon, and Cederbaum, 2009). The roles of both quantum noise and interactions for rotation sensing with bright solitons described by a many-body Schrdinger equation have been analyzed by a variational principle (Haine, 2018). Because of the formation of solitons, enhanced control on the number of atoms N in the experiments can be reached, which is expected to be beneficial for the sensitivity of the interferometry.

The equivalent of a bright soliton in the fully quantum regime of a ring lattice of attracting bosons described by the Bose-Hubbard model was studied by Naldesi *et al.* (2019). Because of the lattice, the soliton and the number of atoms are protected by a finite gap. A barrier can split this "quantum soliton" depending on the interplay among the interaction, number of particles, and barrier strength. For ring-shaped confinement, it was demonstrated that the elementary flux quantum is reduced by $1/N$, where N is the number of particles (Naldesi *et al.*, 2022). This effect potentially yields an N-factor enhancement in the sensitivity of attracting bosons to an external field that can reach the Heisenberg limit (Naldesi *et al.*, 2022; Polo *et al.*, 2022).

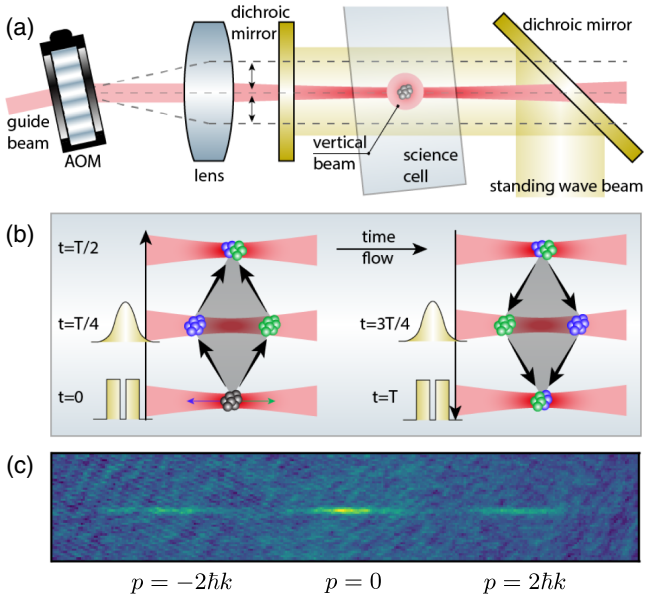

FIG. 10. (a) Experimental setup. (b) Moving waveguide interferometer. The blue and green atoms correspond to the $+2\hbar k$ and $-2\hbar k$ momentum components, respectively. The time flow follows the black arrows. (c) Experimental data acquired $\Delta t =$ 12 ms after the recombination pulse, with atoms in two channels: $|p = 0\rangle$ and $|p = \pm 2\hbar k\rangle$. From Krzyzanowska *et al.*, 2022.

3. Demonstrated atomtronic interferometers

The first compact atom interferometers utilized stationary clouds of ultracold atoms. These devices and some of the notable physics resulting from experiments with them were discussed by Schumm *et al.* (2005), Günther *et al.* (2007), Jo *et al.* (2007), Böhi *et al.* (2009), and Riedel *et al.* (2010). More recently atomtronic interferometers with moving atoms have been realized in both optical and magnetic traps.

An early example is a Michelson interferometer using a BEC propagating over 120 μm in a magnetic waveguide on an atom chip (Wang *et al.*, 2005). Smoother waveguides obtained with larger coils have been used to realize atom interferometers with thermal atoms (Wu, Su, and Prentiss, 2007; Qi *et al.*, 2017) and BECs (Garcia *et al.*, 2006; Burke *et al.*, 2008; Burke and Sackett, 2009). This approach has been used to measure the ground-state polarizability of ^{87}Rb (Deissler *et al.*, 2008). In optical waveguides (Ryu and Boshier, 2015; Akatsuka, Takahashi, and Katori, 2017) linear interferometers extending up to 1 mm have been demonstrated (McDonald, Kuhn *et al.*, 2013). A number of area-enclosing interferometers have been realized in macroscopic magnetic traps (Wu, Su, and Prentiss, 2007; Burke and Sackett, 2009; Qi *et al.*, 2017; Moan *et al.*, 2020).

Recently an atomtronic Sagnac rotation sensor based on a moving linear waveguide formed using a collimated laser beam was demonstrated (Krzyzanowska *et al.*, 2022). The 3.5 mm^2 value enclosed by the atomtronic circuit is the largest result realized to date; see Fig. 10.

In area-enclosing waveguide atom interferometers, the signal can be increased by allowing the wave packets to make multiple orbits around the waveguide loop to increase the enclosed area. The maximum number of round trips is

usually limited by atom loss when the counterpropagating wave packets move through each other. It was recently shown that this limitation can be removed in an interferometer based on a noninteracting ^{39}K BEC, allowing for more than 200 round trips in the guide (Kim *et al.*, 2022).

Note that an atomtronic interferometer can be based on free propagation in a guide (Wang *et al.*, 2005; Akatsuka, Takahashi, and Katori, 2017) or on moving fully trapped atom clouds (clock-type interferometers) (Stevenson *et al.*, 2015; Navez *et al.*, 2016). The first case can be pictured as the atoms functioning as an inertial reference similar to a flywheel. The phase shift occurred by the fully trapped matter waves is perhaps best understood as being based on the relativistic time gains of an atom clock (Hafele and Keating, 1972).

Finally, we note that several other schemes for novel types of atomtronic interferometers have been proposed (Japha *et al.*, 2007; Halkyard, Jones, and Gardiner, 2010; Helm, Cornish, and Gardiner, 2015; Marti, Olf, and Stamper-Kurn, 2015; Helm *et al.*, 2018; Pelegri, Mompart, and Ahufinger, 2018; Moukouri *et al.*, 2021).

V. CONCLUSIONS AND FUTURE PERSPECTIVES

Atomtronics defines micrometer-scale coherent networks to address both technology and basic science. It combines bottom-up and top-down approaches. On the one hand, the circuit elements can be designed to implement the microscopic theory in an experimental realization of unprecedented precision. Just like in electronics, different circuit elements can then be assembled using a hierarchy of heuristic principles. On the other hand, a circuit or even a single circuital element on its own can be used as a current-based quantum simulator to probe the correlated matter.

Important domains of quantum many-body physics in restricted geometries ranging from intermediate to extended spatial scales now become accessible. Analogous to the analysis of current-voltage characteristics in solid-state physics, atomtronic circuits have the potential to define current-based emulators and simulators, effectively widening the scope of the existing ones. Currents, in particular, are the natural quantity to explore not only superflows but also transport in disordered and complex media, as well as topological properties and edge states. An interesting direction to take is to exploit atomtronic circuits to address important questions of high-energy physics, such as the phase diagram of the quark-gluon plasma (He, Jin, and Zhuang, 2006; Rapp *et al.*, 2007; Cazalilla, Ho, and Ueda, 2009; Ozawa and Baym, 2010; Chetcuti *et al.*, 2021) and various scattering process in elementary particle physics (Clark *et al.*, 2017; Fu *et al.*, 2020; Surace and Lerose, 2021). Bosonic rings can be employed to study the dynamics of the expanding Universe (Eckel *et al.*, 2018).

Atomtronic circuitry has a practical potential as well a potential that can be realized in part by leveraging the know-how and heuristic design principles of electronics. Atomtronic triple-well transistors are in many respects close analogs of their electronic field-effect transistor counterparts and can be utilized in matter-wave oscillators to produce matter waves with high spatial coherence (Anderson, 2021), which in turn can carry modulated signals or be used in sensing applications. In the future, one can expect many of the familiar elemental functions of electronic circuitry, such as amplifiers, switches, and oscillators, to be carried over to the quantum regime. In other directions, coupled ring circuits, ring-rectilinear waveguides, etc., have been considered as simple instances of integrated atomtronic circuits (Ryu and Boshier, 2015; Polo, Mompart, and Ahufinger, 2016; Safaei *et al.*, 2019; Pérez-Obiol, Polo, and Amico, 2021).

Building on the theoretically demonstrated qubit dynamics of specific matter-wave circuits (see Sec. IV.D), it will certainly be important to explore atomtronics as a platform for quantum gates. At the same time, matter-wave circuits provide a valuable route to realizing high-precision compact interferometers working on a wide range of sensitivity and in controllable physical conditions. Such devices are of considerable technological importance in different contexts ranging from inertial navigation (Bongs *et al.*, 2019) to geophysics (Jaroszewicz *et al.*, 2016). Unlike their classical or quantum electronic counterparts, atomtronic circuits can operate a regime in which quantum effects can be dominant and long coherence times are possible with a much simpler cryogenics. In this context, experimental, theoretical, and technological inputs are envisaged to be combined together to realize the optimal building block circuit from which complex structures forming actual devices and sensors can be constructed. An important challenge to face in the years to come is to integrate the atomtronic circuits with other existing technologies such as photonic or superconducting integrated circuits (Nirrengarten *et al.*, 2006; Mukai *et al.*, 2007; Cano *et al.*, 2008; Müller *et al.*, 2010a, 2010b; Zhang *et al.*, 2012; Tosto *et al.*, 2019); for hybrid circuits specifically relevant as quantum information, see Fortágh and Zimmermann (2007), Verdú *et al.* (2009), Bernon *et al.* (2013), Xiang *et al.* (2013), Yu, Landra *et al.* (2016, 2018), Yu, Valado *et al.* (2016a, 2016b), Hattermann *et al.* (2017), Yu *et al.* (2017a, 2017b), Yu, Kwek *et al.* (2018), and Petrosyan *et al.* (2019). Such hybrid networks may provide a valuable route for the fabrication of integrated 3D matter-wave circuits in which rectilinear ring guides, beam splitters, etc., together with the fields for the control and readout of the quantum states and the lasers needed for cooling and manipulation of the cold atoms are built into a single chip. Such an approach can be important to achieve scalable matter-wave circuits.

For studies in both fundamental science and circuit design with wider specifications, an interesting future direction would be to expand the investigations to fermionic atomtronic circuits (Cai *et al.*, 2022; Del Pace *et al.*, 2022) or to open the research in the field to new platforms such as fermionic systems with N spin components (Chetcuti *et al.*, 2021; Chetcuti, Haug *et al.*, 2022; Chetcuti, Osterloh *et al.*, 2022) and Rydberg atoms. In the latter platform, bath engineering (Keck, Rossini, and Fazio, 2018; Damanet *et al.*, 2019a, 2019b; Uchino and Brantut, 2020) together with the achieved control of the Rydberg blockade phenomenon (Valado *et al.*, 2016; Simonelli *et al.*, 2017; Archimi *et al.*, 2019) can be explored to start currents with novel specifications. Such a solution may grant access to the realization of fast atomtronic circuits.

ACKNOWLEDGMENTS

We acknowledge the late Frank Hekking for the important contributions given to the atomtronics field from the earliest stages. We thank G. Birkl, P. Bouyer, W. J. Chetcuti, C. Clark, J. Dalibard, R. Dumke, R. Folman, B. Garraway, T. Giamarchi, T. Haug, T. Neely, S. Pandey, H. Perrin, J. Polo-Gomez, C. Sackett, and J. Schmiedmayer for comments and suggestions on the manuscript. We acknowledge fruitful discussions with J. I. Latorre, A. J. Leggett, C. Miniatura, P. Naldesi, G. Pecci, and K. Wright.

REFERENCES

Abad, M., 2016, Phys. Rev. A **93**, 033603.
Abad, M., A. Sartori, S. Finazzi, and A. Recati, 2014, Phys. Rev. A **89**, 053602.
Affleck, I., 1988, Nucl. Phys. **B305**, 582.
Aghamalyan, D., 2015, Ph.D. thesis (National University of Singapore).
Aghamalyan, D., L. Amico, and L. C. Kwek, 2013, Phys. Rev. A **88**, 063627.
Aghamalyan, D., M. Cominotti, M. Rizzi, D. Rossini, F. Hekking, A. Minguzzi, L. C. Kwek, and L. Amico, 2015, New J. Phys. **17**, 045023.
Aghamalyan, D., N. Nguyen, F. Auksztol, K. Gan, M. M. Valado, P. Condylis, L. Kwek, R. Dumke, and L. Amico, 2016, New J. Phys. **18**, 075013.
Aharonov, Y., and D. Bohm, 1959, Phys. Rev. **115**, 485.
Akatsuka, T., T. Takahashi, and H. Katori, 2017, Appl. Phys. Express **10**, 112501.
Albiez, M., R. Gati, J. Fölling, S. Hunsmann, M. Cristiani, and M. K. Oberthaler, 2005, Phys. Rev. Lett. **95**, 010402.
Amico, L., 2000, Mod. Phys. Lett. B **14**, 759.
Amico, L., D. Aghamalyan, F. Auksztol, H. Crepaz, R. Dumke, and L. C. Kwek, 2014, Sci. Rep. **4**, 4298.
Amico, L., G. Birkl, M. Boshier, and L.-C. Kwek, 2017, New J. Phys. **19**, 020201.
Amico, L., and V. Korepin, 2004, Ann. Phys. (N.Y.) **314**, 496.
Amico, L., A. Osterloh, and F. Cataliotti, 2005, Phys. Rev. Lett. **95**, 063201.
Amico, L., and V. Penna, 2000, Phys. Rev. B **62**, 1224.
Amico, L., *et al.*, 2021, AVS Quantum Sci. **3**, 039201.
Anderson, D. Z., 2021, arXiv:2106.10550.
Andersson, E., T. Calarco, R. Folman, M. Andersson, B. Hessmo, and J. Schmiedmayer, 2002, Phys. Rev. Lett. **88**, 100401.
Andrei, N., 1995, *Low-Dimensional Quantum Field Theories for Condensed Matter Physicists* (World Scientific, Singapore), p. 457.
Andrews, M. R., C. G. Townsend, H.-J. Miesner, D. S. Durfee, D. M. Kurn, and W. Ketterle, 1997, Science **275**, 637.
Anoshkin, K., Z. Wu, and E. Zaremba, 2013, Phys. Rev. A **88**, 013609.
Arabahmadi, E., D. Schumayer, and D. A. W. Hutchinson, 2021, Phys. Rev. A **103**, 043319.
Archimi, M., C. Simonelli, L. Di Virgilio, A. Greco, M. Ceccanti, E. Arimondo, D. Ciampini, I. Ryabtsev, I. Beterov, and O. Morsch, 2019, Phys. Rev. A **100**, 030501.
Arimondo, E., W. Ertmer, W. Schleich, and E. Rasel, 2009, *Atom Optics and Space Physics*, Proceedings of the International School of Physics "Enrico Fermi," Course CLXVIII, edited by E. Arimondo, W. Ertmer, E. M. Rasel, and W. P. Schleich (IOS Press, Amsterdam).
Arlt, J., T. Hitomi, and K. Dholakia, 2000, Appl. Phys. B **71**, 549.
Arnold, A. S., C. S. Garvie, and E. Riis, 2006, Phys. Rev. A **73**, 041606.
Arnold, A. S., C. MacCormick, and M. G. Boshier, 2002, Phys. Rev. A **65**, 031601.
Averin, D., and A. Bardas, 1995, Phys. Rev. Lett. **75**, 1831.
Baeriswyl, D., D. K. Campbell, J. M. Carmelo, F. Guinea, and E. Louis, 2013, Eds., *The Hubbard Model: Its Physics and Mathematical Physics*, NATO Science Series B Vol. 343 (Springer Science+Business Media, New York).
Baiborodov, Y. T., M. S. Ioffe, V. M. Petrov, and R. I. Sobolev, 1963, J. Nucl. Energy, Part C **5**, 409.
Barontini, G., R. Labouvie, F. Stubenrauch, A. Vogler, V. Guarrera, and H. Ott, 2013, Phys. Rev. Lett. **110**, 035302.
Barredo, D., V. Lienhard, S. De Leseleuc, T. Lahaye, and A. Browaeys, 2018, Nature (London) **561**, 79.
Beattie, S., S. Moulder, R. J. Fletcher, and Z. Hadzibabic, 2013, Phys. Rev. Lett. **110**, 025301.
Bell, T. A., G. Gauthier, T. W. Neely, H. Rubinsztein-Dunlop, M. J. Davis, and M. A. Baker, 2018, Phys. Rev. A **98**, 013604.
Bell, T. A., J. A. P. Glidden, L. Humbert, M. W. J. Bromley, S. A. Haine, M. J. Davis, T. W. Neely, M. A. Baker, and H. Rubinsztein-Dunlop, 2016, New J. Phys. **18**, 035003.
Bentine, E., T. L. Harte, K. Luksch, A. J. Barker, J. Mur-Petit, B. Yuen, and C. J. Foot, 2017, J. Opt. B **50**, 094002.
Bernon, S., *et al.*, 2013, Nat. Commun. **4**, 2380.
Betz, T., *et al.*, 2011, Phys. Rev. Lett. **106**, 020407.
Binanti, F., K. Furutani, and L. Salasnich, 2021, Phys. Rev. A **103**, 063309.
Birkl, G., F. Buchkremer, R. Dumke, and W. Ertmer, 2001, Opt. Commun. **191**, 67.
Bleszynski-Jayich, A., W. Shanks, B. Peaudecerf, E. Ginossar, Von Oppen, F., L. Glazman, and J. Harris, 2009, Science **326**, 272.
Bloch, I., 2005, Nat. Phys. **1**, 23.
Bloch, I., J. Dalibard, and W. Zwerger, 2008, Rev. Mod. Phys. **80**, 885.
Böhi, P., M. F. Riedel, J. Hoffrogge, J. Reichel, T. W. Hänsch, and P. Treutlein, 2009, Nat. Phys. **5**, 592.
Bongs, K., S. Burger, S. Dettmer, D. Hellweg, J. Arlt, W. Ertmer, and K. Sengstock, 2001, Phys. Rev. A **63**, 031602(R).
Bongs, K., M. Holynski, J. Vovrosh, P. Bouyer, G. Condon, E. Rasel, C. Schubert, W. P. Schleich, and A. Roura, 2019, Nat. Rev. Phys. **1**, 731.
Boyer, V., C. M. Chandrashekar, C. J. Foot, and Z. J. Laczik, 2004, J. Mod. Opt. **51**, 2235.
Boyer, V., R. M. Godun, G. Smirne, D. Cassettari, C. M. Chandrashekar, A. B. Deb, Z. J. Laczik, and C. J. Foot, 2006, Phys. Rev. A **73**, 031402.
Brantut, J.-P., C. Grenier, J. Meineke, D. Stadler, S. Krinner, C. Kollath, T. Esslinger, and A. Georges, 2013, Science **342**, 713.
Brantut, J.-P., J. Meineke, D. Stadler, S. Krinner, and T. Esslinger, 2012, Science **337**, 1069.
Bruderer, M., and W. Belzig, 2012, Phys. Rev. A **85**, 013623.
Buluta, I., and F. Nori, 2009, Science **326**, 108.
Burchianti, A., F. Scazza, A. Amico, G. Valtolina, J. A. Seman, C. Fort, M. Zaccanti, M. Inguscio, and G. Roati, 2018, Phys. Rev. Lett. **120**, 025302.
Burke, J. H. T., B. Deissler, K. J. Hughes, and C. A. Sackett, 2008, Phys. Rev. A **78**, 023619.
Burke, J. H. T., and C. A. Sackett, 2009, Phys. Rev. A **80**, 061603.
Büttiker, M., Y. Imry, and M. Y. Azbel, 1984, Phys. Rev. A **30**, 1982.
Büttiker, M., Y. Imry, and R. Landauer, 1983, Phys. Lett. **96A**, 365.
Byers, N., and C. Yang, 1961, Phys. Rev. Lett. **7**, 46.

Cai, Y., D. G. Allman, P. Sabharwal, and K. C. Wright, 2022, Phys. Rev. Lett. **128**, 150401.
Caldeira, A. O., and A. J. Leggett, 1983, Physica (Amsterdam) **121A**, 587.
Caliga, S. C., C. J. Straatsma, and D. Z. Anderson, 2016, New J. Phys. **18**, 025010.
Caliga, S. C., C. J. Straatsma, and D. Z. Anderson, 2017, New J. Phys. **19**, 013036.
Caliga, S. C., C. J. Straatsma, A. A. Zozulya, and D. Z. Anderson, 2016, New J. Phys. **18**, 015012.
Caliga, S. C., C. J. E. Straatsma, A. A. Zozulya, and D. Z. Anderson, 2012, arXiv:1208.3109.
Calogero, F., and A. Degasperis, 1975, Phys. Rev. A **11**, 265.
Cano, D., B. Kasch, H. Hattermann, R. Kleiner, C. Zimmermann, D. Koelle, and J. Fortágh, 2008, Phys. Rev. Lett. **101**, 183006.
Cappellini, G., *et al.*, 2014, Phys. Rev. Lett. **113**, 120402.
Capponi, S., P. Lecheminant, and K. Totsuka, 2016, Ann. Phys. (N.Y.) **367**, 50.
Cassettari, D., B. Hessmo, R. Folman, T. Maier, and J. Schmiedmayer, 2000, Phys. Rev. Lett. **85**, 5483.
Cazalilla, M. A., R. Citro, T. Giamarchi, E. Orignac, and M. Rigol, 2011, Rev. Mod. Phys. **83**, 1405.
Cazalilla, M. A., A. Ho, and M. Ueda, 2009, New J. Phys. **11**, 103033.
Cazalilla, M. A., and A. M. Rey, 2014, Rep. Prog. Phys. **77**, 124401.
Celi, A., P. Massignan, J. Ruseckas, N. Goldman, I. B. Spielman, G. Juzeliūnas, and M. Lewenstein, 2014, Phys. Rev. Lett. **112**, 043001.
Chakraborty, T., and P. Pietiläinen, 1994, Phys. Rev. B **50**, 8460.
Chetcuti, W. J., T. Haug, L. C. Kwek, and L. Amico, 2022, SciPost Phys. **12**, 033.
Chetcuti, W. J., A. Osterloh, L. Amico, and J. Polo, 2022, arXiv:2206.02807.
Chetcuti, W. J., J. Polo, A. Osterloh, P. Castorina, and L. Amico, 2021, arXiv:2112.06950.
Chien, C.-C., M. Di Ventra, and M. Zwolak, 2014, Phys. Rev. A **90**, 023624.
Choy, T., and F. Haldane, 1982, Phys. Lett. **90A**, 83.
Cirac, J. I., and P. Zoller, 2012, Nat. Phys. **8**, 264.
Clark, L. W., A. Gaj, L. Feng, and C. Chin, 2017, Nature (London) **551**, 356.
Cohen-Tannoudji, C., and S. Reynaud, 1977, J. Phys. B **10**, 345.
Colombe, Y., E. Knyazchyan, O. Morizot, B. Mercier, V. Lorent, and H. Perrin, 2004, Europhys. Lett. **67**, 593.
Cominotti, M., M. Rizzi, D. Rossini, D. Aghamalyan, L. Amico, L. C. Kwek, F. Hekking, and A. Minguzzi, 2015, Eur. Phys. J. Special Topics **224**, 519.
Cominotti, M., D. Rossini, M. Rizzi, F. Hekking, and A. Minguzzi, 2014, Phys. Rev. Lett. **113**, 025301.
Corman, L., L. Chomaz, T. Bienaimé, R. Desbuquois, C. Weitenberg, S. Nascimbene, J. Dalibard, and J. Beugnon, 2014, Phys. Rev. Lett. **113**, 135302.
Corman, L., P. Fabritius, S. Häusler, J. Mohan, L. H. Dogra, D. Husmann, M. Lebrat, and T. Esslinger, 2019, Phys. Rev. A **100**, 053605.
Cornell, E. A., and C. E. Wieman, 2002, Rev. Mod. Phys. **74**, 875.
Couvert, A., M. Jeppesen, T. Kawalec, G. Reinaudi, R. Mathevet, and D. Guéry-Odelin, 2008, Europhys. Lett. **83**, 50001.
Crompvoets, F. M., H. L. Bethlem, R. T. Jongma, and G. Meijer, 2001, Nature (London) **411**, 174.
Cronin, A. D., J. Schmiedmayer, and D. E. Pritchard, 2009, Rev. Mod. Phys. **81**, 1051.
Cuevas, J. C., and E. Scheer, 2017, *Molecular Electronics*, Vol. 15 (World Scientific, Singapore).
Curtis, J. E., B. A. Koss, and D. G. Grier, 2002, Opt. Commun. **207**, 169.
Daley, A., P. Zoller, and B. Trauzettel, 2008, Phys. Rev. Lett. **100**, 110404.
Dalfovo, F., S. Giorgini, L. P. Pitaevskii, and S. Stringari, 1999, Rev. Mod. Phys. **71**, 463.
Dalibard, J., F. Gerbier, G. Juzeliūnas, and P. Öhberg, 2011, Rev. Mod. Phys. **83**, 1523.
Dall, R. G., S. S. Hodgman, M. T. Johnsson, K. G. H. Baldwin, and A. G. Truscott, 2010, Phys. Rev. A **81**, 011602.
Damanet, F., E. Mascarenhas, D. Pekker, and A. J. Daley, 2019a, Phys. Rev. Lett. **123**, 180402.
Damanet, F., E. Mascarenhas, D. Pekker, and A. J. Daley, 2019b, New J. Phys. **21**, 115001.
Danshita, I., and A. Polkovnikov, 2012, Phys. Rev. A **85**, 023638.
David, T., Y. Japha, V. Dikovsky, R. Salem, C. Henkel, and R. Folman, 2008, Eur. Phys. J. D **48**, 321.
Davis, T. J., 1999, J. Opt. B **1**, 408.
Deaver, B. S., and W. M. Fairbank, 1961, Phys. Rev. Lett. **7**, 43.
Degen, C. L., F. Reinhard, and P. Cappellaro, 2017, Rev. Mod. Phys. **89**, 035002.
Deissler, B., K. Hughes, J. Burke, and C. Sackett, 2008, Phys. Rev. A **77**, 031604.
Dekker, N. H., C. S. Lee, V. Lorent, J. H. Thywissen, S. P. Smith, M. Drndić, R. M. Westervelt, and M. Prentiss, 2000, Phys. Rev. Lett. **84**, 1124.
del Campo, A., M. G. Boshier, and A. Saxena, 2014, Sci. Rep. **4**, 5274.
Del Pace, G., W. J. Kwon, M. Zaccanti, G. Roati, and F. Scazza, 2021, Phys. Rev. Lett. **126**, 055301.
Del Pace, G., K. Xhani, A. M. Falconi, M. Fedrizzi, N. Grani, D. H. Rajkov, M. Inguscio, F. Scazza, W. Kwon, and G. Roati, 2022, arXiv:2204.06542.
Denschlag, J., D. Cassettari, A. Chenet, S. Schneider, and J. Schmiedmayer, 1999, Appl. Phys. B **69**, 291.
Denschlag, J., D. Cassettari, and J. Schmiedmayer, 1999, Phys. Rev. Lett. **82**, 2014.
Dikovsky, V., Y. Japha, C. Henkel, and R. Folman, 2005, Eur. Phys. J. D **35**, 87.
Diot, D., Y.-J. Wang, D. Anderson, E. Cornell, R. Saravanan, V. Bright, and M. Prentiss, 2004, *Proceedings of the International Quantum Electronics Conference, San Francisco, 2004* (Optica Publishing Group, Washington, DC), p. 60, 10.1364/IQEC.2004.IME1.
Dowling, J. P., and G. J. Milburn, 2003, Phil. Trans. R. Soc. A **361**, 1655.
Dubessy, R., T. Liennard, P. Pedri, and H. Perrin, 2012, Phys. Rev. A **86**, 011602.
Dubessy, R., J. Polo, H. Perrin, A. Minguzzi, and M. Olshanii, 2021, Phys. Rev. Research **3**, 013098.
Dumke, R., T. Müther, M. Volk, W. Ertmer, and G. Birkl, 2002, Phys. Rev. Lett. **89**, 220402.
Dutta, O., M. Gajda, P. Hauke, M. Lewenstein, D.-S. Lühmann, B. A. Malomed, T. Sowiński, and J. Zakrzewski, 2015, Rep. Prog. Phys. **78**, 066001.
Eckel, S., F. Jendrzejewski, A. Kumar, C. J. Lobb, and G. K. Campbell, 2014, Phys. Rev. X **4**, 031052.
Eckel, S., A. Kumar, T. Jacobson, I. B. Spielman, and G. K. Campbell, 2018, Phys. Rev. X **8**, 021021.

Eckel, S., J. G. Lee, F. Jendrzejewski, C. J. Lobb, G. K. Campbell, and W. T. Hill, 2016, Phys. Rev. A **93**, 063619.
Eckel, S., J. G. Lee, F. Jendrzejewski, N. Murray, C. W. Clark, C. J. Lobb, W. D. Phillips, M. Edwards, and G. K. Campbell, 2014, Nature (London) **506**, 200.
Eller, B., O. Oladehin, D. Fogarty, C. Heller, C. W. Clark, and M. Edwards, 2020, Phys. Rev. A **102**, 063324.
Essler, F. H., H. Frahm, F. Göhmann, A. Klümper, and V. E. Korepin, 2005, *The One-Dimensional Hubbard Model* (Cambridge University Press, Cambridge, England).
Fabre, C. M., P. Cheiney, G. L. Gattobigio, F. Vermersch, S. Faure, R. Mathevet, T. Lahaye, and D. Guéry-Odelin, 2011, Phys. Rev. Lett. **107**, 230401.
Faddeev, L., and L. Takhtajan, 2007, *Hamiltonian Methods in the Theory of Solitons* (Springer Science+Business Media, New York).
Fazio, R., and Van Der Zant, H., 2001, Phys. Rep. **355**, 235.
Fernholz, T., R. Gerritsma, S. Whitlock, I. Barb, and R. J. C. Spreeuw, 2008, Phys. Rev. A **77**, 033409.
Filippone, M., F. Hekking, and A. Minguzzi, 2016, Phys. Rev. A **93**, 011602.
Fisher, M. P., P. B. Weichman, G. Grinstein, and D. S. Fisher, 1989, Phys. Rev. B **40**, 546.
Folman, R., P. Krüger, D. Cassettari, B. Hessmo, T. Maier, and J. Schmiedmayer, 2000, Phys. Rev. Lett. **84**, 4749.
Folman, R., P. Krüger, J. Schmiedmayer, J. Denschlag, and C. Henkel, 2002, in *Advances in Atomic, Molecular, and Optical Physics*, Vol. 48, edited by B. Bederson and H. Walther (Elsevier, New York), pp. 263–356.
Fortágh, J., and C. Zimmermann, 2007, Rev. Mod. Phys. **79**, 235.
Franke-Arnold, S., J. Leach, M. Padgett, V. Lembessis, D. Ellinas, A. Wright, J. Girkin, P. Ohberg, and A. Arnold, 2007, Opt. Express **15**, 8619.
Friedman, N., A. Kaplan, D. Carasso, and N. Davidson, 2001, Phys. Rev. Lett. **86**, 1518.
Frye, K., *et al.*, 2021, Eur. Phys. J. Quantum Technol. **8**, 1.
Fu, H., Z. Zhang, K.-X. Yao, L. Feng, J. Yoo, L. W. Clark, K. Levin, and C. Chin, 2020, Phys. Rev. Lett. **125**, 183003.
Gallego-Marcos, F., G. Platero, C. Nietner, G. Schaller, and T. Brandes, 2014, Phys. Rev. A **90**, 033614.
Gallemí, A., M. Guilleumas, M. Richard, and A. Minguzzi, 2018, Phys. Rev. B **98**, 104502.
Garcia, O., B. Deissler, K. J. Hughes, J. M. Reeves, and C. A. Sackett, 2006, Phys. Rev. A **74**, 031601.
Garraway, B. M., and H. Perrin, 2016, J. Opt. B **49**, 172001.
Gati, R., B. Hemmerling, J. Fölling, M. Albiez, and M. K. Oberthaler, 2006, Phys. Rev. Lett. **96**, 130404.
Gattobigio, G. L., A. Couvert, G. Reinaudi, B. Georgeot, and D. Guéry-Odelin, 2012, Phys. Rev. Lett. **109**, 030403.
Gaunt, A. L., and Z. Hadzibabic, 2012, Sci. Rep. **2**, 721.
Gauthier, G., T. A. Bell, A. B. Stilgoe, M. Baker, H. Rubinsztein-Dunlop, and T. W. Neely, 2021, in *Advances in Atomic, Molecular, and Optical Physics*, Vol. 70, edited by L. F. Dimauro, H. Perrin, and S. F. Yelin (Elsevier, New York), p. 1.
Gauthier, G., I. Lenton, N. M. Parry, M. Baker, M. Davis, H. Rubinsztein-Dunlop, and T. Neely, 2016, Optica **3**, 1136.
Gauthier, G., S. S. Szigeti, M. T. Reeves, M. Baker, T. A. Bell, H. Rubinsztein-Dunlop, M. J. Davis, and T. W. Neely, 2019, Phys. Rev. Lett. **123**, 260402.
Gefen, Y., Y. Imry, and M. Y. Azbel, 1984, Phys. Rev. Lett. **52**, 129.
Gehr, R., J. Volz, G. Dubois, T. Steinmetz, Y. Colombe, B. L. Lev, R. Long, J. Esteve, and J. Reichel, 2010, Phys. Rev. Lett. **104**, 203602.
Geiger, R., A. Landragin, S. Merlet, and F. Pereira Dos Santos, 2020, AVS Quantum Sci. **2**, 024702.
Geiger, R., *et al.*, 2011, Nat. Commun. **2**, 474.
Giamarchi, T., 2003, *Quantum Physics in One Dimension*, Vol. 121 (Clarendon Press, Oxford).
Giovanazzi, S., J. Esteve, and M. K. Oberthaler, 2008, New J. Phys. **10**, 045009.
Giovanazzi, S., A. Smerzi, and S. Fantoni, 2000, Phys. Rev. Lett. **84**, 4521.
Goldman, N., G. Juzeliūnas, P. Öhberg, and I. B. Spielman, 2014, Rep. Prog. Phys. **77**, 126401.
Grenier, C., A. Georges, and C. Kollath, 2014, Phys. Rev. Lett. **113**, 200601.
Grenier, C., C. Kollath, and A. Georges, 2016, C.R. Phys. **17**, 1161.
Grimm, R., M. Weidemüller, and Y. B. Ovchinnikov, 2000, in *Advances in Atomic, Molecular, and Optical Physics*, Vol. 42, edited by B. Bederson and H. Walther (Academic Press, New York), pp. 95–170.
Gring, M., M. Kuhnert, T. Langen, T. Kitagawa, B. Rauer, M. Schreitl, I. Mazets, D. A. Smith, E. Demler, and J. Schmiedmayer, 2012, Science **337**, 1318.
Gritsev, V., A. Polkovnikov, and E. Demler, 2007, Phys. Rev. B **75**, 174511.
Guan, X.-W., M. T. Batchelor, and C. Lee, 2013, Rev. Mod. Phys. **85**, 1633.
Guarrera, V., R. Moore, A. Bunting, T. Vanderbruggen, and Y. B. Ovchinnikov, 2017, Sci. Rep. **7**, 4749.
Guerin, W., J.-F. Riou, J. P. Gaebler, V. Josse, P. Bouyer, and A. Aspect, 2006, Phys. Rev. Lett. **97**, 200402.
Günther, A., S. Kraft, C. Zimmermann, and J. Fortágh, 2007, Phys. Rev. Lett. **98**, 140403.
Guo, Y., R. Dubessy, M. de Goër de Herve, A. Kumar, T. Badr, A. Perrin, L. Longchambon, and H. Perrin, 2020, Phys. Rev. Lett. **124**, 025301.
Gupta, S., K. Murch, K. Moore, T. Purdy, and D. Stamper-Kurn, 2005, Phys. Rev. Lett. **95**, 143201.
Gustavson, T. L., P. Bouyer, and M. A. Kasevich, 1997, Phys. Rev. Lett. **78**, 2046.
Gustavson, T. L., A. Landragin, and M. A. Kasevich, 2000, Classical Quantum Gravity **17**, 2385.
Gutiérrez-Medina, B., 2013, Am. J. Phys. **81**, 104.
Gutman, D. B., Y. Gefen, and A. D. Mirlin, 2012, Phys. Rev. B **85**, 125102.
Gutzwiller, M. C., 1963, Phys. Rev. Lett. **10**, 159.
Ha, L.-C., L. W. Clark, C. V. Parker, B. M. Anderson, and C. Chin, 2015, Phys. Rev. Lett. **114**, 055301.
Hafele, J. C., and R. E. Keating, 1972, Science **177**, 168.
Haine, S. A., 2018, New J. Phys. **20**, 033009.
Haldane, F., 1980, Phys. Lett. **80A**, 281.
Halkyard, P. L., M. P. A. Jones, and S. A. Gardiner, 2010, Phys. Rev. A **81**, 061602(R).
Hallwood, D. W., K. Burnett, and J. Dunningham, 2006, New J. Phys. **8**, 180.
Hallwood, D. W., K. Burnett, and J. Dunningham, 2007, J. Mod. Opt. **54**, 2129.
Hallwood, D. W., T. Ernst, and J. Brand, 2010, Phys. Rev. A **82**, 063623.
Hänsel, W., P. Hommelhoff, T. Hänsch, and J. Reichel, 2001, Nature (London) **413**, 498.
Haroche, S., and J.-M. Raimond, 2006, *Exploring the Quantum: Atoms, Cavities, and Photons* (Oxford University Press, New York).
Hattermann, H., D. Bothner, L. Ley, B. Ferdinand, D. Wiedmaier, L. Sárkány, R. Kleiner, D. Koelle, and J. Fortágh, 2017, Nat. Commun. **8**, 2254.

Haug, T., L. Amico, R. Dumke, and L.-C. Kwek, 2018, Quantum Sci. Technol. **3**, 035006.
Haug, T., R. Dumke, L.-C. Kwek, and L. Amico, 2019a, Quantum Sci. Technol. **4**, 045001.
Haug, T., R. Dumke, L.-C. Kwek, and L. Amico, 2019b, Commun. Phys. **2**, 127.
Haug, T., R. Dumke, L.-C. Kwek, C. Miniatura, and L. Amico, 2021, Phys. Rev. Research **3**, 013034.
Haug, T., H. Heimonen, R. Dumke, L.-C. Kwek, and L. Amico, 2019, Phys. Rev. A **100**, 041601.
Haug, T., J. Tan, M. Theng, R. Dumke, L.-C. Kwek, and L. Amico, 2018, Phys. Rev. A **97**, 013633.
Häusler, S., P. Fabritius, J. Mohan, M. Lebrat, L. Corman, and T. Esslinger, 2021, Phys. Rev. X **11**, 021034.
Häusler, S., S. Nakajima, M. Lebrat, D. Husmann, S. Krinner, T. Esslinger, and J.-P. Brantut, 2017, Phys. Rev. Lett. **119**, 030403.
He, L., M. Jin, and P. Zhuang, 2006, Phys. Rev. A **74**, 033604.
Hekking, F., and L. Glazman, 1997, Phys. Rev. B **55**, 6551.
Helm, J., S. Rooney, C. Weiss, and S. Gardiner, 2014, Phys. Rev. A **89**, 033610.
Helm, J. L., T. P. Billam, and S. A. Gardiner, 2012, Phys. Rev. A **85**, 053621.
Helm, J. L., T. P. Billam, A. Rakonjac, S. L. Cornish, and S. A. Gardiner, 2018, Phys. Rev. Lett. **120**, 063201.
Helm, J. L., S. L. Cornish, and S. A. Gardiner, 2015, Phys. Rev. Lett. **114**, 134101.
Henderson, K., C. Ryu, C. MacCormick, and M. G. Boshier, 2009, New J. Phys. **11**, 043030.
Henkel, C., P. Kruger, R. Folman, and J. Schmiedmayer, 2003, Appl. Phys. B **76**, 173.
Hod, O., R. Baer, and E. Rabani, 2006, Phys. Rev. Lett. **97**, 266803.
Hodby, E., G. Hechenblaikner, O. M. Marago, J. Arlt, S. Hopkins, and C. J. Foot, 2000, J. Phys. B **33**, 4087.
Hofferberth, S., I. Lesanovsky, B. Fischer, T. Schumm, and J. Schmiedmayer, 2007, Nature (London) **449**, 324.
Hofferberth, S., I. Lesanovsky, B. Fischer, J. Verdu, and J. Schmiedmayer, 2006, Nat. Phys. **2**, 710.
Hofferberth, S., I. Lesanovsky, T. Schumm, A. Imambekov, V. Gritsev, E. Demler, and J. Schmiedmayer, 2008, Nat. Phys. **4**, 489.
Houde, O., D. Kadio, and L. Pruvost, 2000, Phys. Rev. Lett. **85**, 5543.
Hubbard, J., 1963, Proc. R. Soc. A **276**, 238.
Hueck, K., A. Mazurenko, N. Luick, T. Lompe, and H. Moritz, 2017, Rev. Sci. Instrum. **88**, 016103.
Husmann, D., M. Lebrat, S. Häusler, J.-P. Brantut, L. Corman, and T. Esslinger, 2018, Proc. Natl. Acad. Sci. U.S.A. **115**, 8563.
Husmann, D., S. Uchino, S. Krinner, M. Lebrat, T. Giamarchi, T. Esslinger, and J.-P. Brantut, 2015, Science **350**, 1498.
Hyafil, P., J. Mozley, A. Perrin, J. Tailleur, G. Nogues, M. Brune, J. M. Raimond, and S. Haroche, 2004, Phys. Rev. Lett. **93**, 103001.
Imry, Y., 2002, *Introduction to Mesoscopic Physics* (Oxford University Press, New York).
Imry, Y., and R. Landauer, 1999, Rev. Mod. Phys. **71**, S306.
Ivanov, A., G. Kordas, A. Komnik, and S. Wimberger, 2013, Eur. Phys. J. B **86**, 345.
Jagla, E., and C. Balseiro, 1993, Phys. Rev. Lett. **70**, 639.
Jaksch, D., C. Bruder, J. I. Cirac, C. W. Gardiner, and P. Zoller, 1998, Phys. Rev. Lett. **81**, 3108.
Japha, Y., O. Arzouan, Y. Avishai, and R. Folman, 2007, Phys. Rev. Lett. **99**, 060402.
Jaroszewicz, L. R., A. Kurzych, Z. Krajewski, P. Marć, J. K. Kowalski, P. Bobra, Z. Zembaty, B. Sakowicz, and R. Jankowski, 2016, Sensors **16**, 2161.
Jendrzejewski, F., S. Eckel, N. Murray, C. Lanier, M. Edwards, C. J. Lobb, and G. K. Campbell, 2014, Phys. Rev. Lett. **113**, 045305.
Jo, G. B., J. H. Choi, C. A. Christensen, T. A. Pasquini, Y. R. Lee, W. Ketterle, and D. E. Pritchard, 2007, Phys. Rev. Lett. **98**, 180401.
Jördens, R., N. Strohmaier, K. Günter, H. Moritz, and T. Esslinger, 2008, Nature (London) **455**, 204.
Kanamori, J., 1963, Prog. Theor. Phys. **30**, 275.
Kanász-Nagy, M., L. Glazman, T. Esslinger, and E. A. Demler, 2016, Phys. Rev. Lett. **117**, 255302.
Keck, M., D. Rossini, and R. Fazio, 2018, Phys. Rev. A **98**, 053812.
Keil, M., O. Amit, S. Zhou, D. Groswasser, Y. Japha, and R. Folman, 2016, J. Mod. Opt. **63**, 1840.
Ketterle, W., 2002, Rev. Mod. Phys. **74**, 1131.
Khondker, A., M. R. Khan, and A. Anwar, 1988, J. Appl. Phys. **63**, 5191.
Kim, H., K. Krzyzanowska, K. C. Henderson, C. Ryu, E. Timmermans, and M. Boshier, 2022, arXiv:22201.11888.
Kim, S. J., H. Yu, S. T. Gang, and J. B. Kim, 2017, Appl. Phys. B **123**, 154.
Kolovsky, A. R., 2017, Phys. Rev. A **96**, 011601.
Kolovsky, A. R., Z. Denis, and S. Wimberger, 2018, Phys. Rev. A **98**, 043623.
Korepin, V. E., N. M. Bogoliubov, and A. G. Izergin, 1997, *Quantum Inverse Scattering Method and Correlation Functions*, Vol. 3 (Cambridge University Press, Cambridge, England).
Kovachy, T., J. M. Hogan, A. Sugarbaker, S. M. Dickerson, C. A. Donnelly, C. Overstreet, and M. A. Kasevich, 2015, Phys. Rev. Lett. **114**, 143004.
Kraft, S., A. Günther, H. Ott, D. Wharam, C. Zimmermann, and J. Fortágh, 2002, J. Opt. B **35**, L469.
Kreutzmann, H., U. V. Poulsen, M. Lewenstein, R. Dumke, W. Ertmer, G. Birkl, and A. Sanpera, 2004, Phys. Rev. Lett. **92**, 163201.
Krinner, S., T. Esslinger, and J.-P. Brantut, 2017, J. Phys. Condens. Matter **29**, 343003.
Krinner, S., M. Lebrat, D. Husmann, C. Grenier, J.-P. Brantut, and T. Esslinger, 2016, Proc. Natl. Acad. Sci. U.S.A. **113**, 8144.
Krinner, S., D. Stadler, D. Husmann, J.-P. Brantut, and T. Esslinger, 2015, Nature (London) **517**, 64.
Krinner, S., D. Stadler, J. Meineke, J.-P. Brantut, and T. Esslinger, 2013, Phys. Rev. Lett. **110**, 100601.
Krinner, S., D. Stadler, J. Meineke, J.-P. Brantut, and T. Esslinger, 2015, Phys. Rev. Lett. **115**, 045302.
Krüger, P., L. M. Andersson, S. Wildermuth, S. Hofferberth, E. Haller, S. Aigner, S. Groth, I. Bar-Joseph, and J. Schmiedmayer, 2007, Phys. Rev. A **76**, 063621.
Krzyzanowska, K., J. Ferreras, C. Ryu, E. C. Samson, and M. Boshier, 2022, arXiv:22201.12461.
Kuga, T., Y. Torii, N. Shiokawa, T. Hirano, Y. Shimizu, and H. Sasada, 1997, Phys. Rev. Lett. **78**, 4713.
Kumar, A., N. Anderson, W. D. Phillips, S. Eckel, G. K. Campbell, and S. Stringari, 2016, New J. Phys. **18**, 025001.
Kumar, A., S. Eckel, F. Jendrzejewski, and G. K. Campbell, 2017, Phys. Rev. A **95**, 021602.
Kunimi, M., and I. Danshita, 2017, Phys. Rev. A **95**, 033637.
Kunimi, M., and I. Danshita, 2019, Phys. Rev. A **99**, 043613.
Kwon, W. J., G. Del Pace, R. Panza, M. Inguscio, W. Zwerger, M. Zaccanti, F. Scazza, and G. Roati, 2020, Science **369**, 84.
Labouvie, R., B. Santra, S. Heun, S. Wimberger, and H. Ott, 2015, Phys. Rev. Lett. **115**, 050601.
Lacki, M., M. Baranov, H. Pichler, and P. Zoller, 2016, Phys. Rev. Lett. **117**, 233001.

Lamata, L., A. Mezzacapo, J. Casanova, and E. Solano, 2014, Eur. Phys. J. Quantum Technol. **1**, 9.
Langen, T., R. Geiger, and J. Schmiedmayer, 2015, Annu. Rev. Condens. Matter Phys. **6**, 201.
Lau, J. W. Z., K. S. Gan, R. Dumke, L. Amico, L.-C. Kwek, and T. Haug, 2022, arXiv:2205.01636.
Leanhardt, A., A. Chikkatur, D. Kielpinski, Y. Shin, T. Gustavson, W. Ketterle, and D. Pritchard, 2002, Phys. Rev. Lett. **89**, 040401.
LeBlanc, L. J., A. B. Bardon, J. McKeever, M. H. T. Extavour, D. Jervis, J. H. Thywissen, F. Piazza, and A. Smerzi, 2011, Phys. Rev. Lett. **106**, 025302.
Lebrat, M., P. Grišins, D. Husmann, S. Häusler, L. Corman, T. Giamarchi, J.-P. Brantut, and T. Esslinger, 2018, Phys. Rev. X **8**, 011053.
Lebrat, M., S. Häusler, P. Fabritius, D. Husmann, L. Corman, and T. Esslinger, 2019, Phys. Rev. Lett. **123**, 193605.
Lee, T. D., K. Huang, and C. N. Yang, 1957, Phys. Rev. **106**, 1135.
Leggett, A., 2006, *Quantum Fluids* (Oxford University Press, Oxford).
Leggett, A. J., 1980, Prog. Theor. Phys. Suppl. **69**, 80.
Leggett, A. J., 1991, NATO ASI Ser., Ser. B **251**, 297.
Lesanovsky, I., and W. von Klitzing, 2007, Phys. Rev. Lett. **99**, 083001.
Levy, S., E. Lahoud, I. Shomroni, and J. Steinhauer, 2007, Nature (London) **449**, 579.
Lévy, L. P., G. Dolan, J. Dunsmuir, and H. Bouchiat, 1990, Phys. Rev. Lett. **64**, 2074.
Lewenstein, M., A. Sanpera, and V. Ahufinger, 2012, *Ultracold Atoms in Optical Lattices: Simulating Quantum Many-Body Systems* (Oxford University Press, New York).
Li, A., S. Eckel, B. Eller, K. E. Warren, C. W. Clark, and M. Edwards, 2016, Phys. Rev. A **94**, 023626.
Li, G., M. D. Fraser, A. Yakimenko, and E. A. Ostrovskaya, 2015, Phys. Rev. B **91**, 184518.
Lieb, E. H., and W. Liniger, 1963, Phys. Rev. **130**, 1605.
Lieb, E. H., and F. Wu, 1968, Phys. Rev. Lett. **21**, 192.
Lim, Y., J. Goo, H. Kwak, and Y. Shin, 2021, Phys. Rev. A **103**, 063319.
Liu, B., H. Zhai, and S. Zhang, 2017, Phys. Rev. A **95**, 013623.
Lobos, A., and A. Aligia, 2008, Phys. Rev. Lett. **100**, 016803.
Long, R., T. Rom, W. Hansel, T. W. Hansch, and J. Reichel, 2005, Eur. Phys. J. D **35**, 125.
Loss, D., 1992, Phys. Rev. Lett. **69**, 343.
Luick, N., L. Sobirey, M. Bohlen, V. P. Singh, L. Mathey, T. Lompe, and H. Moritz, 2020, Science **369**, 89.
Lukoshkin, V. A., V. K. Kalevich, M. M. Afanasiev, K. V. Kavokin, Z. Hatzopoulos, P. G. Savvidis, E. S. Sedov, and A. V. Kavokin, 2018, Phys. Rev. B **97**, 195149.
Mahan, G. D., 2013, *Many-Particle Physics* (Springer Science+ Business Media, New York).
Majorana, E., 1932, Nuovo Cimento **9**, 43.
Manmana, S. R., K. R. Hazzard, G. Chen, A. E. Feiguin, and A. M. Rey, 2011, Phys. Rev. A **84**, 043601.
Marchukov, O. V., B. A. Malomed, V. A. Yurovsky, M. Olshanii, V. Dunjko, and R. G. Hulet, 2019, Phys. Rev. A **99**, 063623.
Marino, I., S. Raghavan, S. Fantoni, S. R. Shenoy, and A. Smerzi, 1999, Phys. Rev. A **60**, 487.
Marquardt, F., and C. Bruder, 2002, Phys. Rev. B **65**, 125315.
Marti, G. E., R. Olf, and D. M. Stamper-Kurn, 2015, Phys. Rev. A **91**, 013602.
Mas, H., S. Pandey, G. Vasilakis, and W. von Klitzing, 2019, New J. Phys. **21**, 123039.
Mathew, R., A. Kumar, S. Eckel, F. Jendrzejewski, G. K. Campbell, M. Edwards, and E. Tiesinga, 2015, Phys. Rev. A **92**, 033602.
Mathey, A. C., C. W. Clark, and L. Mathey, 2014, Phys. Rev. A **90**, 023604.
Mathey, A. C., and L. Mathey, 2016, New J. Phys. **18**, 055016.
Matveev, K., A. Larkin, and L. Glazman, 2002, Phys. Rev. Lett. **89**, 096802.
McDonald, G. D., H. Keal, P. A. Altin, J. E. Debs, S. Bennetts, C. C. N. Kuhn, K. S. Hardman, M. T. Johnsson, J. D. Close, and N. P. Robins, 2013, Phys. Rev. A **87**, 013632.
McDonald, G. D., C. C. Kuhn, K. S. Hardman, S. Bennetts, P. J. Everitt, P. A. Altin, J. E. Debs, J. D. Close, and N. P. Robins, 2014, Phys. Rev. Lett. **113**, 013002.
McDonald, G. D., C. C. N. Kuhn, S. Bennetts, J. E. Debs, K. S. Hardman, M. Johnsson, J. D. Close, and N. P. Robins, 2013, Phys. Rev. A **88**, 053620.
McGloin, D., G. C. Spalding, H. Melville, W. Sibbett, and K. Dholakia, 2003, Opt. Express **11**, 158.
Mehdi, Z., A. S. Bradley, J. J. Hope, and S. S. Szigeti, 2021, SciPost Phys. **11**, 80.
Meier, F., and W. Zwerger, 2001, Phys. Rev. A **64**, 033610.
Mielke, A., 2015, in *Many Body Physics: From Kondo to Hubbard*, Vol. 5, edited by P. Coleman, E. Koch, and E. Pavarini (Verlag des Forschungszentrum Jülich, Jülich, Germany).
Milburn, G., J. Corney, E. M. Wright, and D. Walls, 1997, Phys. Rev. A **55**, 4318.
Milner, V., J. L. Hanssen, W. C. Campbell, and M. G. Raizen, 2001, Phys. Rev. Lett. **86**, 1514.
Moan, E. R., R. A. Horne, T. Arpornthip, Z. Luo, A. J. Fallon, S. J. Berl, and C. A. Sackett, 2020, Phys. Rev. Lett. **124**, 120403.
Mohanty, P., 1999, Ann. Phys. (Berlin) **511**, 549.
Morizot, O., Y. Colombe, V. Lorent, H. Perrin, and B. M. Garraway, 2006, Phys. Rev. A **74**, 023617.
Moukouri, S., Y. Japha, M. Keil, T. David, D. Groswasser, M. Givon, and R. Folman, 2021, arXiv:22107.03446.
Moulder, S., S. Beattie, R. P. Smith, N. Tammuz, and Z. Hadzibabic, 2012, Phys. Rev. A **86**, 013629.
Mukai, T., C. Hufnagel, A. Kasper, T. Meno, A. Tsukada, K. Semba, and F. Shimizu, 2007, Phys. Rev. Lett. **98**, 260407.
Müller, D., D. Z. Anderson, R. J. Grow, P. D. D. Schwindt, and E. A. Cornell, 1999, Phys. Rev. Lett. **83**, 5194.
Müller, D., E. A. Cornell, D. Z. Anderson, and E. R. I. Abraham, 2000, Phys. Rev. A **61**, 033411.
Müller, D., E. A. Cornell, M. Prevedelli, P. Schwindt, A. Zozulya, and D. Z. Anderson, 2000, Opt. Lett. **25**, 1382.
Müller, H., S.-w. Chiow, Q. Long, S. Herrmann, and S. Chu, 2008, Phys. Rev. Lett. **100**, 180405.
Müller, T., B. Zhang, R. Fermani, K. Chan, M. Lim, and R. Dumke, 2010a, Phys. Rev. A **81**, 053624.
Müller, T., B. Zhang, R. Fermani, K. Chan, Z. Wang, C. Zhang, M. Lim, and R. Dumke, 2010b, New J. Phys. **12**, 043016.
Müllers, A., B. Santra, C. Baals, J. Jiang, J. Benary, R. Labouvie, D. A. Zezyulin, V. V. Konotop, and H. Ott, 2018, Sci. Adv. **4**, eaat6539.
Muntinga, H., *et al.*, 2013, Phys. Rev. Lett. **110**, 093602.
Murray, N., M. Krygier, M. Edwards, K. C. Wright, G. K. Campbell, and C. W. Clark, 2013, Phys. Rev. A **88**, 053615.
Naldesi, P., J. P. Gomez, B. Malomed, M. Olshanii, A. Minguzzi, and L. Amico, 2019, Phys. Rev. Lett. **122**, 053001.
Naldesi, P., J. Polo, V. Dunjko, H. Perrin, M. Olshanii, L. Amico, and A. Minguzzi, 2022, SciPost Phys. **12**, 138.

Navez, P., S. Pandey, H. Mas, K. Poulios, T. Fernholz, and W. von Klitzing, 2016, New J. Phys. **18**, 075014.
Nazarov, Y. V., and Y. M. Blanter, 2009, *Quantum Transport: Introduction to Nanoscience* (Cambridge University Press, Cambridge, England).
Nicolau, E., J. Mompart, B. Juliá-Diaz, and V. Ahufinger, 2020, Phys. Rev. A **102**, 023331.
Nietner, C., G. Schaller, and T. Brandes, 2014, Phys. Rev. A **89**, 013605.
Nirrengarten, T., A. Qarry, C. Roux, A. Emmert, G. Nogues, M. Brune, J.-M. Raimond, and S. Haroche, 2006, Phys. Rev. Lett. **97**, 200405.
Nitzan, A., and M. A. Ratner, 2003, Science **300**, 1384.
Nogrette, F., H. Labuhn, S. Ravets, D. Barredo, L. Béguin, A. Vernier, T. Lahaye, and A. Browaeys, 2014, Phys. Rev. X **4**, 021034.
Nunnenkamp, A., A. M. Rey, and K. Burnett, 2008, Phys. Rev. A **77**, 023622.
Nunnenkamp, A., A. M. Rey, and K. Burnett, 2011, Phys. Rev. A **84**, 053604.
Oelkers, N., and J. Links, 2007, Phys. Rev. B **75**, 115119.
Olariu, S., and I. I. Popescu, 1985, Rev. Mod. Phys. **57**, 339.
Oliinyk, A., A. Yakimenko, and B. Malomed, 2019, J. Phys. B **52**, 225301.
Olson, S. E., M. L. Terraciano, M. Bashkansky, and F. K. Fatemi, 2007, Phys. Rev. A **76**, 061404.
Onofrio, R., D. S. Durfee, C. Raman, M. Kohl, C. E. Kuklewicz, and W. Ketterle, 2000, Phys. Rev. Lett. **84**, 810.
Ozawa, T., and G. Baym, 2010, Phys. Rev. A **82**, 063615.
Packard, R. E., 1998, Rev. Mod. Phys. **70**, 641.
Pagano, G., M. Mancini, G. Cappellini, L. Livi, C. Sias, J. Catani, M. Inguscio, and L. Fallani, 2015, Phys. Rev. Lett. **115**, 265301.
Pandey, S., H. Mas, G. Drougakis, P. Thekkeppatt, V. Bolpasi, G. Vasilakis, K. Poulios, and W. von Klitzing, 2019, Nature (London) **570**, 205.
Pandey, S., H. Mas, G. Vasilakis, and W. von Klitzing, 2021, Phys. Rev. Lett. **126**, 170402.
Papoular, D. J., L. P. Pitaevskii, and S. Stringari, 2014, Phys. Rev. Lett. **113**, 170601.
Papoular, D. J., L. P. Pitaevskii, and S. Stringari, 2016, Phys. Rev. A **94**, 023622.
Pâţu, O. I., and D. V. Averin, 2022, Phys. Rev. Lett. **128**, 096801.
Pecci, G., P. Naldesi, L. Amico, and A. Minguzzi, 2021, Phys. Rev. Research **3**, L032064.
Pecci, G., P. Naldesi, A. Minguzzi, and L. Amico, 2021, arXiv:2105.10408.
Peierls, R., 1933, Z. Phys. **80**, 763.
Pelegri, G., J. Mompart, and V. Ahufinger, 2018, New J. Phys. **20**, 103001.
Penna, V., and A. Richaud, 2017, Phys. Rev. A **96**, 053631.
Pepino, R., J. Cooper, D. Anderson, and M. Holland, 2009, Phys. Rev. Lett. **103**, 140405.
Pepino, R. A., 2021, Entropy **23**, 534.
Pérez-Obiol, A., J. Polo, and L. Amico, 2021, arXiv:2112.08072.
Perrin, H., and B. M. Garraway, 2017, in *Advances in Atomic, Molecular, and Optical Physics*, Vol. 66, edited by S. Yelin, E. Arimondo, and C. Lin (Elsevier, New York).
Pershoguba, S. S., and L. I. Glazman, 2019, Phys. Rev. B **99**, 134514.
Peters, A., K. Y. Chung, and S. Chu, 2001, Metrologia **38**, 25.
Petrich, W., M. H. Anderson, J. R. Ensher, and E. A. Cornell, 1995, Phys. Rev. Lett. **74**, 3352.
Petrosyan, D., K. Mølmer, J. Fortágh, and M. Saffman, 2019, New J. Phys. **21**, 073033.
Pezzè, L., A. Smerzi, M. K. Oberthaler, R. Schmied, and P. Treutlein, 2018, Rev. Mod. Phys. **90**, 035005.
Piazza, F., L. A. Collins, and A. Smerzi, 2009, Phys. Rev. A **80**, 021601(R).
Pigneur, M., T. Berrada, M. Bonneau, T. Schumm, E. Demler, and J. Schmiedmayer, 2018, Phys. Rev. Lett. **120**, 173601.
Polo, J., and V. Ahufinger, 2013, Phys. Rev. A **88**, 053628.
Polo, J., V. Ahufinger, F. W. Hekking, and A. Minguzzi, 2018, Phys. Rev. Lett. **121**, 090404.
Polo, J., A. Benseny, T. Busch, V. Ahufinger, and J. Mompart, 2016, New J. Phys. **18**, 015010.
Polo, J., R. Dubessy, P. Pedri, H. Perrin, and A. Minguzzi, 2019, Phys. Rev. Lett. **123**, 195301.
Polo, J., J. Mompart, and V. Ahufinger, 2016, Phys. Rev. A **93**, 033613.
Polo, J., P. Naldesi, A. Minguzzi, and L. Amico, 2022, Quantum Sci. Technol. **7**, 015015.
Price, H. M., T. Ozawa, and N. Goldman, 2017, Phys. Rev. A **95**, 023607.
Pritchard, D. E., 1983, Phys. Rev. Lett. **51**, 1336.
Pritchard, J. D., A. N. Dinkelaker, A. S. Arnold, P. F. Griffin, and E. Riis, 2012, New J. Phys. **14**, 103047.
Pyykkönen, V. A. J., S. Peotta, P. Fabritius, J. Mohan, T. Esslinger, and P. Törmä, 2021, Phys. Rev. B **103**, 144519.
Qi, L., Z. Hu, T. Valenzuela, Y. Zhang, Y. Zhai, W. Quan, N. Waltham, and J. Fang, 2017, Appl. Phys. Lett. **110**, 153502.
Ramanathan, A., K. C. Wright, S. R. Muniz, M. Zelan, W. T. Hill, C. J. Lobb, K. Helmerson, W. D. Phillips, and G. K. Campbell, 2011, Phys. Rev. Lett. **106**, 130401.
Rapp, A., G. Zaránd, C. Honerkamp, and W. Hofstetter, 2007, Phys. Rev. Lett. **98**, 160405.
Rastelli, G., I. M. Pop, and F. W. Hekking, 2013, Phys. Rev. B **87**, 174513.
Read, N., and N. Cooper, 2003, Phys. Rev. A **68**, 035601.
Reichel, J., 2002, Appl. Phys. B **74**, 469.
Reichel, J., W. Hänsel, and T. W. Hänsch, 1999, Phys. Rev. Lett. **83**, 3398.
Reichel, J., and V. Vuletić, 2011, *Atom Chips* (Wiley-VCH, Weinheim).
Renn, M. J., E. A. Donley, E. A. Cornell, C. E. Wieman, and D. Z. Anderson, 1996, Phys. Rev. A **53**, R648.
Rhodes, D. P., G. P. T. Lancaster, J. Livesey, D. McGloin, J. Arlt, and K. Dholakia, 2002, Opt. Commun. **214**, 247.
Richaud, A., M. Ferraretto, and M. Capone, 2021, Phys. Rev. B **103**, 205132.
Richaud, A., M. Ferraretto, and M. Capone, 2022, Condens. Matter **7**, 18.
Richaud, A., and V. Penna, 2017, Phys. Rev. A **96**, 013620.
Riedel, E. K., and F. von Oppen, 1993, Phys. Rev. B **47**, 15449.
Riedel, M. F., P. Böhi, Y. Li, T. W. Hänsch, A. Sinatra, and P. Treutlein, 2010, Nature (London) **464**, 1170.
Rincón, J., A. Aligia, and K. Hallberg, 2009, Phys. Rev. B **79**, 035112.
Rincón, J., K. Hallberg, and A. Aligia, 2008, Phys. Rev. B **78**, 125115.
Roscilde, T., M. F. Faulkner, S. T. Bramwell, and P. C. W. Holdsworth, 2016, New J. Phys. **18**, 075003.
Rubinsztein-Dunlop, H., *et al.*, 2017, J. Opt. **19**, 013001.
Ruostekoski, J., and D. F. Walls, 1998, Phys. Rev. A **58**, R50.
Ryu, C., P. Blackburn, A. Blinova, and M. Boshier, 2013, Phys. Rev. Lett. **111**, 205301.
Ryu, C., and M. G. Boshier, 2015, New J. Phys. **17**, 092002.
Ryu, C., K. C. Henderson, and M. G. Boshier, 2014, New J. Phys. **16**, 013046.

Ryu, C., E. C. Samson, and M. G. Boshier, 2020, Nat. Commun. **11**, 3338.
Safaei, S., B. Grémaud, R. Dumke, L.-C. Kwek, L. Amico, and C. Miniatura, 2018, Phys. Rev. A **97**, 042306.
Safaei, S., L.-C. Kwek, R. Dumke, and L. Amico, 2019, Phys. Rev. A **100**, 013621.
Salerno, G., H. M. Price, M. Lebrat, S. Häusler, T. Esslinger, L. Corman, J.-P. Brantut, and N. Goldman, 2019, Phys. Rev. X **9**, 041001.
Salim, E. A., S. C. Caliga, J. B. Pfeiffer, and D. Z. Anderson, 2013, Appl. Phys. Lett. **102**, 084104.
Saminadayar, L., C. Bauerle, and D. Mailly, 2004, Encycl. Nanosci. Nanotechnol. **3**, 267.
Sanvitto, D., *et al.*, 2010, Nat. Phys. **6**, 527.
Sauer, J. A., M. D. Barrett, and M. S. Chapman, 2001, Phys. Rev. Lett. **87**, 270401.
Schenke, C., A. Minguzzi, and F. W. J. Hekking, 2011, Phys. Rev. A **84**, 053636.
Schmiedmayer, J., 1995a, Phys. Rev. A **52**, R13.
Schmiedmayer, J., 1995b, Appl. Phys. B **60**, 169.
Schmiedmayer, J., and A. Scrinzi, 1996a, Quantum Semiclass. Opt. **8**, 693.
Schmiedmayer, J., and A. Scrinzi, 1996b, Phys. Rev. A **54**, R2525.
Schneble, D., M. Hasuo, T. Anker, T. Pfau, and J. Mlynek, 2003, J. Opt. Soc. Am. B **20**, 648.
Schnelle, S. K., E. D. Van Ooijen, M. J. Davis, N. R. Heckenberg, and H. Rubinsztein-Dunlop, 2008, Opt. Express **16**, 1405.
Schumm, T., S. Hofferberth, L. M. Andersson, S. Wildermuth, S. Groth, I. Bar-Joseph, J. Schmiedmayer, and P. Krüger, 2005, Nat. Phys. **1**, 57.
Schweigler, T., *et al.*, 2021, Nat. Phys. **17**, 559.
Seaman, B., M. Krämer, D. Anderson, and M. Holland, 2007, Phys. Rev. A **75**, 023615.
Sekera, T., C. Bruder, and W. Belzig, 2016, Phys. Rev. A **94**, 033618.
Sherlock, B. E., M. Gildemeister, E. Owen, E. Nugent, and C. J. Foot, 2011, Phys. Rev. A **83**, 043408.
Shmakov, P., A. Dmitriev, and V. Y. Kachorovskii, 2013, Phys. Rev. B **87**, 235417.
Simonelli, C., M. Archimi, L. Asteria, D. Capecchi, G. Masella, E. Arimondo, D. Ciampini, and O. Morsch, 2017, Phys. Rev. A **96**, 043411.
Simpson, D., D. Gangardt, I. Lerner, and P. Krüger, 2014, Phys. Rev. Lett. **112**, 100601.
Sinclair, C. D. J., E. A. Curtis, I. L. Garcia, J. A. Retter, B. V. Hall, S. Eriksson, B. E. Sauer, and E. A. Hinds, 2005, Phys. Rev. A **72**, 031603.
Singh, V. P., N. Luick, L. Sobirey, and L. Mathey, 2020, Phys. Rev. Research **2**, 033298.
Sinuco-León, G. A., K. A. Burrows, A. S. Arnold, and B. M. Garraway, 2014, Nat. Commun. **5**, 5289.
Smerzi, A., S. Fantoni, S. Giovanazzi, and S. Shenoy, 1997, Phys. Rev. Lett. **79**, 4950.
Solenov, D., and D. Mozyrsky, 2010, Phys. Rev. A **82**, 061601.
Sommer, A., M. Ku, G. Roati, and M. W. Zwierlein, 2011, Nature (London) **472**, 201.
Spagnolli, G., *et al.*, 2017, Phys. Rev. Lett. **118**, 230403.
Spehner, D., L. Morales-Molina, and S. A. Reyes, 2021, New J. Phys. **23**, 063025.
Stadler, D., S. Krinner, J. Meineke, J.-P. Brantut, and T. Esslinger, 2012, Nature (London) **491**, 736.
Stevenson, R., M. R. Hush, T. Bishop, I. Lesanovsky, and T. Fernholz, 2015, Phys. Rev. Lett. **115**, 163001.
Stickney, J. A., D. Z. Anderson, and A. A. Zozulya, 2007, Phys. Rev. A **75**, 013608.
Stockton, J., K. Takase, and M. Kasevich, 2011, Phys. Rev. Lett. **107**, 133001.
Streltsov, A. I., O. E. Alon, and L. S. Cederbaum, 2009, Phys. Rev. A **80**, 043616.
Sugarbaker, A., 2014, Ph.D. thesis (Stanford University).
Sun, K., K. Padavić, F. Yang, S. Vishveshwara, and C. Lannert, 2018, Phys. Rev. A **98**, 013609.
Surace, F. M., and A. Lerose, 2021, New J. Phys. **23**, 062001.
Sutherland, B., 1968, Phys. Rev. Lett. **20**, 98.
Sutherland, B., 1975, Phys. Rev. B **12**, 3795.
Tajik, M., B. Rauer, T. Schweigler, F. Cataldini, J. Sabino, F. S. Møller, S.-C. Ji, I. E. Mazets, and J. Schmiedmayer, 2019, Opt. Express **27**, 33474.
Thouless, D., 1983, Phys. Rev. B **27**, 6083.
Thouless, D. J., M. Kohmoto, M. P. Nightingale, and M. den Nijs, 1982, Phys. Rev. Lett. **49**, 405.
Tinkham, M., 2012, *Introduction to Superconductivity* (Courier Dover Publications, Mineola, NY).
Tokuno, A., M. Oshikawa, and E. Demler, 2008, Phys. Rev. Lett. **100**, 140402.
Tollett, J. J., C. C. Bradley, C. A. Sackett, and R. G. Hulet, 1995, Phys. Rev. A **51**, R22.
Tononi, A., F. Toigo, S. Wimberger, A. Cappellaro, and L. Salasnich, 2020, New J. Phys. **22**, 073020.
Tosto, F., P. Baw Swe, N. T. Nguyen, C. Hufnagel, M. Martínez Valado, L. Prigozhin, V. Sokolovsky, and R. Dumke, 2019, Appl. Phys. Lett. **114**, 222601.
Trebbia, J.-B., C. L. Garrido Alzar, R. Cornelussen, C. I. Westbrook, and I. Bouchoule, 2007, Phys. Rev. Lett. **98**, 263201.
Trenkwalder, A., *et al.*, 2016, Nat. Phys. **12**, 826.
Turpin, A., J. Polo, Y. V. Loiko, J. Küber, F. Schmaltz, T. K. Kalkandjiev, V. Ahufinger, G. Birkl, and J. Mompart, 2015, Opt. Express **23**, 1638.
Uchino, S., 2020, Phys. Rev. Research **2**, 023340.
Uchino, S., and J.-P. Brantut, 2020, Phys. Rev. Research **2**, 023284.
Uchino, S., and M. Ueda, 2017, Phys. Rev. Lett. **118**, 105303.
Uchino, S., M. Ueda, and J.-P. Brantut, 2018, Phys. Rev. A **98**, 063619.
Vaidman, L., 2012, Phys. Rev. A **86**, 040101.
Valado, M., C. Simonelli, M. Hoogerland, I. Lesanovsky, J. P. Garrahan, E. Arimondo, D. Ciampini, and O. Morsch, 2016, Phys. Rev. A **93**, 040701.
Valtolina, G., F. Scazza, A. Amico, A. Burchianti, A. Recati, T. Enss, M. Inguscio, M. Zaccanti, and G. Roati, 2017, Nat. Phys. **13**, 704.
Valtolina, G., *et al.*, 2015, Science **350**, 1505.
van Wees, B. J., H. van Houten, C. W. J. Beenakker, J. G. Williamson, L. P. Kouwenhoven, D. van der Marel, and C. T. Foxon, 1988, Phys. Rev. Lett. **60**, 848.
van Zoest, T., *et al.*, 2010, Science **328**, 1540.
Verdú, J., H. Zoubi, C. Koller, J. Majer, H. Ritsch, and J. Schmiedmayer, 2009, Phys. Rev. Lett. **103**, 043603.
Victorin, N., T. Haug, L.-C. Kwek, L. Amico, and A. Minguzzi, 2019, Phys. Rev. A **99**, 033616.
Waintal, X., G. Fleury, K. Kazymyrenko, M. Houzet, P. Schmitteckert, and D. Weinmann, 2008, Phys. Rev. Lett. **101**, 106804.
Wang, Y., S. Subhankar, P. Bienias, M. Lacki, T.-C. Tsui, M. A. Baranov, A. V. Gorshkov, P. Zoller, J. V. Porto, and S. L. Rolston, 2018, Phys. Rev. Lett. **120**, 083601.

Wang, Y.-H., A. Kumar, F. Jendrzejewski, R. M. Wilson, M. Edwards, S. Eckel, G. K. Campbell, and C. W. Clark, 2015, New J. Phys. **17**, 125012.
Wang, Y.-J., D. Z. Anderson, V. M. Bright, E. A. Cornell, Q. Diot, T. Kishimoto, M. Prentiss, R. A. Saravanan, S. R. Segal, and S. Wu, 2005, Phys. Rev. Lett. **94**, 090405.
Watabe, S., and Y. Kato, 2008, Phys. Rev. A **78**, 063611.
Webb, R. A., S. Washburn, C. Umbach, and R. Laibowitz, 1985, Phys. Rev. Lett. **54**, 2696.
Weiss, C., and Y. Castin, 2009, Phys. Rev. Lett. **102**, 010403.
Wharam, D. A., T. J. Thornton, R. Newbury, M. Pepper, H. Ahmed, J. E. F. Frost, D. G. Hasko, D. C. Peacock, D. A. Ritchie, and G. A. C. Jones, 1988, J. Phys. C **21**, L209.
White, D. H., T. A. Haase, D. J. Brown, M. D. Hoogerland, M. S. Najafabadi, J. L. Helm, C. Gies, D. Schumayer, and D. A. W. Hutchinson, 2020, Nat. Commun. **11**, 4942.
Wright, E., J. Arlt, and K. Dholakia, 2000, Phys. Rev. A **63**, 013608.
Wright, K. C., R. B. Blakestad, C. J. Lobb, W. D. Phillips, and G. K. Campbell, 2013a, Phys. Rev. Lett. **110**, 025302.
Wright, K. C., R. B. Blakestad, C. J. Lobb, W. D. Phillips, and G. K. Campbell, 2013b, Phys. Rev. A **88**, 063633.
Wu, S., E. Su, and M. Prentiss, 2007, Phys. Rev. Lett. **99**, 173201.
Wu, S., Y.-J. Wang, Q. Diot, and M. Prentiss, 2005, Phys. Rev. A **71**, 043602.
Xhani, K., *et al.*, 2020, Phys. Rev. Lett. **124**, 045301.
Z.-L. Xiang, S. Ashhab, J. Q. You, and F. Nori, 2013, Rev. Mod. Phys. **85**, 623.
Yakimenko, A., Y. Bidasyuk, M. Weyrauch, Y. Kuriatnikov, and S. Vilchinskii, 2015, Phys. Rev. A **91**, 033607.
Yakimenko, A., S. Vilchinskii, Y. Bidasyuk, Y. Kuriatnikov, K. Isaieva, and M. Weyrauch, 2014, arXiv:1411.3490.
Yao, J., B. Liu, M. Sun, and H. Zhai, 2018, Phys. Rev. A **98**, 041601.
You, J.-S., R. Schmidt, D. A. Ivanov, M. Knap, and E. Demler, 2019, Phys. Rev. B **99**, 214505.
Yu, D., L. C. Kwek, L. Amico, and R. Dumke, 2017a, Quantum Sci. Technol. **2**, 035005.
Yu, D., L. C. Kwek, L. Amico, and R. Dumke, 2017b, Phys. Rev. A **95**, 053811.
Yu, D., L. C. Kwek, L. Amico, and R. Dumke, 2018, Phys. Rev. A **98**, 033833.
Yu, D., A. Landra, L. C. Kwek, L. Amico, and R. Dumke, 2018, New J. Phys. **20**, 023031.
Yu, D., A. Landra, M. M. Valado, C. Hufnagel, L. C. Kwek, L. Amico, and R. Dumke, 2016, Phys. Rev. A **94**, 062301.
Yu, D., M. M. Valado, C. Hufnagel, L. C. Kwek, L. Amico, and R. Dumke, 2016a, Phys. Rev. A **93**, 042329.
Yu, D., M. M. Valado, C. Hufnagel, L. C. Kwek, L. Amico, and R. Dumke, 2016b, Sci. Rep. **6**, 38356.
Yu, N., and M. Fowler, 1992, Phys. Rev. B **45**, 11795.
Zabow, G., R. S. Conroy, and M. G. Prentiss, 2004, Phys. Rev. Lett. **92**, 180404.
Zaccanti, M., and W. Zwerger, 2019, Phys. Rev. A **100**, 063601.
Zapata, I., and F. Sols, 2009, Phys. Rev. Lett. **102**, 180405.
Zapata, I., F. Sols, and A. J. Leggett, 1998, Phys. Rev. A **57**, R28.
Zhang, B., M. Siercke, K. S. Chan, M. Beian, M. J. Lim, and R. Dumke, 2012, Phys. Rev. A **85**, 013404.
Zobay, O., and B. M. Garraway, 2001, Phys. Rev. Lett. **86**, 1195.
Zöllner, S., H.-D. Meyer, and P. Schmelcher, 2008, Phys. Rev. Lett. **100**, 040401.
Zou, Y. Q., E. Le Cerf, B. Bakkali-Hassani, C. Maury, G. Chauveau, P. C. M. Castilho, R. Saint-Jalm, S. Nascimbene, J. Dalibard, and J. Beugnon, 2021, J. Opt. B **54**, 08LT01.
Zozulya, A. A., and D. Z. Anderson, 2013, Phys. Rev. A **88**, 043641.
Zupancic, P., P. M. Preiss, R. Ma, A. Lukin, M. E. Tai, M. Rispoli, R. Islam, and M. Greiner, 2016, Opt. Express **24**, 13881.
Zvyagin, A. A., and I. V. Krive, 1995, Low Temp. Phys. **21**, 533.